

Large violation of Leggett–Garg inequalities with coherent-state projectors for a harmonic oscillator and chiral scalar field

Tomoya Hirotani,^{1,*} Akira Matsumura,^{1,†} Yasusada Nambu,^{2,‡} and Kazuhiro Yamamoto^{1,§}

¹*Department of Physics, Kyushu University, 744 Motooka, Nishi-Ku, Fukuoka 819-0395, Japan*

²*Department of Physics, Graduate School of Science, Nagoya University, Chikusa, Nagoya 464-8602, Japan*

(Dated: January 30, 2024)

We investigate violations of Leggett–Garg inequalities (LGIs) for a harmonic oscillator and a $(1+1)$ -dimensional chiral scalar field with coherent-state projectors, which is equivalent to a heterodyne-type measurement scheme. For the harmonic oscillator, we found that the vacuum and thermal states violated the LGIs by evaluating the two-time quasi-probability distribution function. In particular, we demonstrate that the value of the two-time quasi-probability reaches -0.123 for a squeezed coherent-state projector, which is equivalent to 98% of the Lüders bound corresponding to the maximal violation of the LGIs. We also find a violation of the LGIs for the local mode of a quantum chiral scalar field by constructing a coherent-state projector similar to the harmonic oscillator case. In contrast to the harmonic oscillator, the periodicity in the time direction of the quasi-probability disappears, which is related to the existence of quantum entanglement between the local mode and its complementary degrees of freedom.

I. INTRODUCTION

How can we be sure that a system is quantum mechanical? Violation of macroscopic realism (MR) is a concept that characterizes quantum mechanics. In a classical system, the state of an object exists even before the measurement is made. However, in quantum mechanical systems, it is not necessarily true that an object is fixed in a particular state before observation. How can we check whether MR is broken? Leggett–Garg inequalities (LGIs) were proposed by Leggett and Garg in 1985 to test whether a macroscopic system follows MR [1]. According to Halliwell [2], the necessary and sufficient condition for MR to be valid is the existence of 12 two-time LGIs and 4 three-time LGIs, for a total of 16 LGIs. In other words, if any of the 16 LGIs are violated, we can confirm that MR does not hold in that system. If MR does not hold, we can conclude that the system is quantum. Conversely, note that we cannot conclude that there is no quantumness in a system in which MR appears to hold; that is, all 16 LGIs hold true.

In MR theory, for a dichotomic variable $Q(t)$ that takes definite values of ± 1 , we consider the sequential measurement of Q at times t_1 and t_2 . Then, the following inequalities hold:

$$(1 + s_1 Q(t_1))(1 + s_2 Q(t_2)) \geq 0, \quad (1)$$

where $s_1 = \pm 1$ and $s_2 = \pm 1$. Following the MR framework, a joint probability distribution function exists for the measurement results, and the existence of such a joint probability implies that we can simply average the above formula and obtain two-time LGIs:

$$1 + s_1 \langle Q_1 \rangle + s_2 \langle Q_2 \rangle + s_1 s_2 \langle Q_1 Q_2 \rangle \geq 0, \quad (2)$$

where $Q_1 := Q(t_1)$, $Q_2 := Q(t_2)$, and $\langle \cdot \rangle$ denotes the ensemble averages of the measurement results. In quantum mechanics, the above expression is promoted to be positivity of the two-time quasi-probability defined by

$$q_{s_1 s_2} := \frac{1}{4} \left(1 + s_1 \langle \hat{Q}_1 \rangle + s_2 \langle \hat{Q}_2 \rangle + \frac{1}{2} s_1 s_2 \langle \{\hat{Q}_1, \hat{Q}_2\} \rangle \right) = \text{ReTr} \left[\hat{M}_{s_2}(t_2) \hat{M}_{s_1}(t_1) \hat{\rho}_0 \right], \quad (3)$$

where $\hat{M}_s = (1 + s\hat{Q})/2$ is the projector (measurement operator) for the dichotomic operator \hat{Q} and $\hat{\rho}_0$ is the quantum state of the target system. The two-time LGIs are equivalent to $q_{s_1 s_2} \geq 0$ and the negativities of the quasi-probability indicate a violation of MR (violation of the LGIs).

* hirotani.tomoya.937@s.kyushu-u.ac.jp

† matsumura.akira@phys.kyushu-u.ac.jp

‡ nambu@gravity.phys.nagoya-u.ac.jp

§ yamamoto@phys.kyushu-u.ac.jp

In terms of the expected values of the dichotomic operator, the quasi-probability is

$$q_{s_1 s_2} = \frac{1}{8} \left\langle (1 + s_1 \hat{Q}_1 + s_2 \hat{Q}_2)^2 - 1 \right\rangle \geq -\frac{1}{8}. \quad (4)$$

This quantity is always positive for classical systems, and its negativity implies a violation of MR. The minimum value $-1/8$ is called the Lüders bound [3], which corresponds to the maximal violation of the LGIs. To verify the LGIs experimentally, we obtain the expectation values $\langle \hat{Q}_{1,2} \rangle$ and $\langle \hat{Q}_1 \hat{Q}_2 \rangle$ from the experimental data and then check whether the quasi-probability (3) is negative.

The two-time probabilities for these sequential measurements are

$$p_{12}(s_1, s_2) := \text{Tr} \left[\hat{M}_{s_2}(t_2) \hat{M}_{s_1}(t_1) \hat{\rho}_0 \hat{M}_{s_1}(t_1) \right], \quad (5)$$

which is a manifestly positively valued quantity but does not satisfy the following no-signaling-in-time condition (NSIT) [4–6]:

$$p_2(s_2) := \text{Tr} \left[\hat{M}_{s_2}(t_2) \hat{\rho}_0 \right] = \sum_{s_1} p_{12}(s_1, s_2). \quad (6)$$

For a pure initial state $\rho_0 = |\psi_0\rangle \langle \psi_0|$, p_{12} fails to satisfy the probability sum rule because of the interference between the pairs of states $|\psi_+\rangle = \hat{M}_+(t_2) \hat{M}_{s_1}(t_1) |\psi_0\rangle$ and $|\psi_-\rangle = \hat{M}_-(t_2) \hat{M}_{s_1}(t_1) |\psi_0\rangle$. Although the quasi-probability formally satisfies the probability sum rule

$$p_2(s_2) = \sum_{s_1} q_{s_1 s_2}, \quad (7)$$

the value of quasi-probability can become negative, which implies quantum mechanical behavior of the system.

As typical systems, LGIs are specifically applied to quantum-harmonic oscillators (QHOs) [7–11]. Assuming that the dichotomic variable \hat{Q} is in the form of a sign function indicates that the quasi-probability for the ground state of a QHO does not violate both the two-time LGIs and the three-time LGIs [8]. However, by making the dichotomic operator a more coarse-grained or nontrivial form [11], even for the ground state, there are some cases in which the LGIs are violated; we will confirm this behavior in this study. This implies that the features of the measurement operator must be carefully considered when verifying MR of the system. In previous studies, LGIs have been applied to various types of Gaussian states: coherent, thermal, squeezed, squeezed coherent, and thermally squeezed coherent [7–11]. With the settings of [9], the violation of the LGIs reached 84% of the Lüders bound [3], which provided the maximal value of the violation of the LGIs. Moreover, using a different scheme with temporal correlations (called no-signaling in time) has shown that violations of MR can be verified independently of the mass, momentum, and frequency of the QHO [10]. Experimental verification of LGIs has been reported in [12–14], mainly using qubit systems. Although there are few analyses of LGIs applied to quantum fields, Tani et al. [15] investigated the LGIs for $(3+1)$ -dimensional quantum fields and $(1+1)$ -dimensional chiral massless scalar fields, and they concluded that, for the vacuum state of the field, no violation of the LGIs occurred without adopting a nontrivial dichotomic variable \hat{Q} .

In this study, we investigated the violation of LGIs for harmonic oscillator and chiral scalar field systems with coherent-state measurements. As a dichotomic observable for the LGIs, we adopted one defined via a Gaussian projector (Gaussian POVM) [9, 10]. We will see that the Gaussian projector results in a greater violation of the LGIs compared to non-Gaussian-type projectors (e.g., $\hat{Q} = \text{sgn}(\hat{x})$ [7–9, 11]). For the scalar field system, we introduced a local oscillator mode assigned to a specified spatial region from the scalar field using a window function. This window function was selected to respect the symplectic structure of the local mode. Because the local mode is defined as an oscillator embedded in the total quantum field system, its state becomes mixed and evolves in a nonunitary manner. Therefore, we do not have a Hamiltonian that determines the evolution of the local mode required to evaluate the projectors at specified times. To overcome this difficulty, we express the local mode operators using the creation and annihilation operators of the original quantum field and take the summation over each wavenumber mode to obtain the quasi-probability of the local mode.

The remainder of this paper is organized as follows: In Sec. II, we present the violation of the LGIs for a harmonic oscillator with a Gaussian projector, and we explain why the LGIs are violated in comparison with the classical motion of the oscillator. In Sec. III, we consider the LGIs in a $(1+1)$ -dimensional chiral scalar field and derive a formula for the quasi-probability of the spatial local modes of the scalar field. We found that the LGIs violated the suitable projector parameters. We also discuss the LGI experiment using quantum Hall systems. Section IV is devoted to a summary and conclusions. Throughout this paper, we adopt the unit $c = \hbar = 1$.

II. VIOLATION OF LGI FOR A HARMONIC OSCILLATOR SYSTEM

A. Harmonic oscillator system

Let us consider the quasi-probability in a harmonic oscillator system [7–11] with the following Hamiltonian:

$$\hat{H} = \frac{\hat{p}^2}{2} + \frac{\Omega^2}{2}\hat{q}^2 = \Omega \left(\hat{a}^\dagger \hat{a} + \frac{1}{2} \right), \quad (8)$$

where \hat{p} and \hat{q} are the dimensionless momentum and position operators, respectively, and Ω is the angular frequency of the harmonic oscillator. The annihilation and creation operators are defined as

$$\hat{a} = \sqrt{\frac{\Omega}{2}} \hat{q} + \frac{i}{\sqrt{2\Omega}} \hat{p}, \quad \hat{a}^\dagger = \sqrt{\frac{\Omega}{2}} \hat{q} - \frac{i}{\sqrt{2\Omega}} \hat{p}. \quad (9)$$

The oscillator ground state is defined as $\hat{a}|0\rangle = 0$. For this ground state, each expectation value is calculated as $\langle \hat{q} \rangle = \langle \hat{p} \rangle = 0$, $\langle \hat{q}^2 \rangle = 1/(2\Omega)$, and $\langle \hat{p}^2 \rangle = \Omega/2$. The coherent state of the oscillator is defined as

$$|\alpha\rangle = e^{\alpha\hat{a}^\dagger - \alpha^* \hat{a}} |0\rangle = \hat{D}_a(\alpha) |0\rangle = e^{-|\alpha|^2/2} \sum_n \frac{\alpha^n}{\sqrt{n!}} |n\rangle, \quad (10)$$

where $\hat{D}_a(\alpha)$ denotes the displacement operator. With the evolution operator $\hat{U}(t) = \exp(-i\hat{H}t)$, the coherent state evolves into

$$\hat{U}(t) |\alpha\rangle = e^{-i\Omega t/2} |e^{-i\Omega t}\alpha\rangle, \quad \hat{U}^\dagger \hat{a} \hat{U} = e^{-i\Omega t} \hat{a}. \quad (11)$$

For the initial state of the oscillator, we assume a thermally coherent state

$$\hat{\rho}_0 = C \hat{D}_a(\alpha) \exp(-A\hat{a}^\dagger \hat{a}) \hat{D}_a^\dagger(\alpha), \quad \text{Tr} \hat{\rho}_0 = 1, \quad (12)$$

with the normalization $C = (\text{Tr} \exp(-A\hat{a}^\dagger \hat{a}))^{-1} = (1 - e^{-A})$. The constant A is related to the symplectic eigenvalue ν of the covariance matrix for the Gaussian state (12) as follows:

$$e^{-A} = \frac{\nu - 1/2}{\nu + 1/2}, \quad \nu^2 = \langle \hat{q}^2 \rangle \langle \hat{p}^2 \rangle \geq \frac{1}{4}. \quad (13)$$

The temperature T of the thermal state is related to ν by $\nu^{-1} = 2 \tanh(\Omega/(2T))$.¹ In the zero-temperature limit, $T \rightarrow 0$, $\nu = 1/2$ and $\hat{\rho}_0$ becomes a pure state.

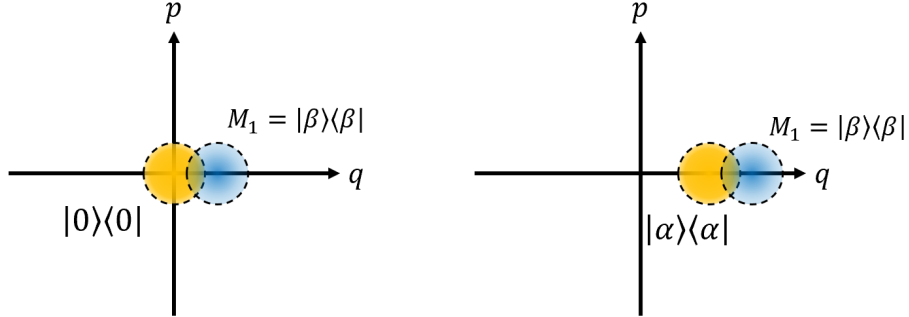


FIG. 1. Schematic plot of the coherent-state measurement of the vacuum state $|0\rangle$ (left panel) and the coherent state $|\alpha\rangle$ (right panel). The dashed circles represent 1σ contours of the Gaussian state. As the measurement result, we assign the dichotomic variable $Q = +1$ if the obtained measurement result (q, p) is included in the blue disks; otherwise, $Q = -1$. After the measurement, the state $|\alpha\rangle \langle \alpha|$ of the target system is projected to $|\langle \alpha | \beta \rangle|^2 |\beta\rangle \langle \beta|$ if the measurement result is $Q = +1$.

¹ We can use the following formula to express the thermal state in terms of the displacement operator:

$$e^{-A\hat{a}^\dagger \hat{a}} = \frac{1}{(\nu + 1/2)\pi} \int d^2 z e^{-\nu|z|^2} \hat{D}_a(z), \quad \nu = \frac{1}{2} \left(\frac{1 + e^{-A}}{1 - e^{-A}} \right).$$

B. Measurement operator

As discussed extensively in [16], violation of conventional LGIs is equivalent to the existence of negative values of quasi-probability defined by

$$q_{s_1 s_2} = \text{ReTr} \left[\hat{M}_{s_2}(t_2) \hat{M}_{s_1}(t_1) \hat{\rho}_0 \right], \quad (14)$$

where \hat{M}_s is the measurement operator for a dichotomic observable \hat{Q} with the specified measurement results $s = \pm 1$ and $\hat{\rho}_0$ denotes the initial state of the target oscillator. In terms of \hat{Q} , the measurement operator is expressed as

$$\hat{M}_s = \frac{1 + s \hat{Q}}{2}, \quad \hat{Q}^2 = 1, \quad s = \pm 1. \quad (15)$$

We consider LGIs with generalized measurements by adopting the following Gaussian measurement operators [17]

$$\hat{M}_s = \frac{1 - s}{2} + s |\beta_b\rangle \langle \beta_b| = \begin{cases} |\beta_b\rangle \langle \beta_b| & \text{for } s = +1, \\ 1 - |\beta_b\rangle \langle \beta_b| & \text{for } s = -1, \end{cases} \quad (16)$$

where $|\beta_b\rangle$ is the coherent state with the annihilation operator defined by

$$\hat{b} := \sqrt{\frac{\omega}{2}} \hat{q} + \frac{i}{\sqrt{2\omega}} \hat{p} = \cosh r \hat{a} + \sinh r \hat{a}^\dagger, \quad e^r = \sqrt{\frac{\omega}{\Omega}}, \quad (17)$$

where ω is the angular frequency of the projector (a measurement apparatus parameter). This type of measurement operator maps Gaussian states to Gaussian states and can be realized experimentally by appending ancillary modes initialized in Gaussian states, implementing Gaussian unitary operations on the system and ancillary modes, and measuring quadrature operators that can be achieved using balanced homodyne detection in the optics framework. The annihilation operator is expressed as $\hat{b} = \hat{S}^\dagger(r) \hat{a} \hat{S}(r)$ with the squeezing operator

$$\hat{S}(\zeta) = \exp \left(\frac{\zeta}{2} \hat{a}^{\dagger 2} - \frac{\zeta^*}{2} \hat{a}^2 \right), \quad \zeta = r e^{i\varphi}, \quad (18)$$

where ζ is the squeezing parameter and φ is the constant phase. The “vacuum state” defined by \hat{b} is determined as $\hat{b} |0_b\rangle = 0$ with $|0_b\rangle = \hat{S}^{-1}(r) |0\rangle$, where $\hat{a} |0\rangle = 0$. Hence

$$|\beta_b\rangle = e^{\beta \hat{b}^\dagger - \beta^* \hat{b}} \hat{S}(-r) |0\rangle = \hat{D}_a(\gamma) \hat{S}(e^{i\pi} r) |0\rangle =: |\gamma, \zeta\rangle, \quad \gamma = \beta \cosh r - \beta^* \sinh r, \quad \zeta = e^{i\pi} r. \quad (19)$$

Therefore, $|\beta_b\rangle$ is the squeezed coherent state $|\gamma, \zeta\rangle$ with displacement parameter γ and squeezing parameter ζ . Parameters β , r , and ω in the projector (16) are regarded as the measurement parameters. The evolution of the projector $\hat{M}_1 = |\beta_b\rangle \langle \beta_b|$ is

$$\begin{aligned} \hat{M}_1(t) &= \hat{U}^\dagger(t) \hat{M}_1 \hat{U}(t) \\ &= \hat{U}^\dagger(t) \hat{D}(\gamma) \hat{S}(\zeta) |0\rangle \langle 0| \hat{S}^\dagger(\zeta) \hat{D}^\dagger(\gamma) \hat{U}(t) \\ &= \hat{D}(e^{i\Omega t} \gamma) \hat{S}(e^{2i\Omega t} \zeta) |0\rangle \langle 0| \hat{S}^\dagger(e^{2i\Omega t} \zeta) \hat{D}^\dagger(e^{i\Omega t} \gamma) \\ &= |e^{i\Omega t} \gamma, e^{2i\Omega t} \zeta\rangle \langle e^{i\Omega t} \gamma, e^{2i\Omega t} \zeta|. \end{aligned} \quad (20)$$

The projector with measurement result s is

$$\hat{M}_s(t) = \frac{1 - s}{2} + s |\gamma(t), \zeta(t)\rangle \langle \gamma(t), \zeta(t)|, \quad \gamma(t) = e^{i\Omega t} \gamma, \quad \zeta(t) = e^{2i\Omega t + i\pi} r. \quad (21)$$

If we adopt the dichotomic operator $\hat{Q} = 2 |\beta\rangle \langle \beta| - 1$, where $|\beta\rangle$ is a coherent state, then the measurement operator for this dichotomic operator is $\hat{M}_1 = |\beta\rangle \langle \beta|$ and $\hat{M}_{-1} = 1 - |\beta\rangle \langle \beta|$ (Fig. 1). Hence for the vacuum state of the target oscillator, if the measurement result with a fixed s is $+1$, this implies $Q = +1$; on the other hand, if the measurement result is -1 , this implies $Q = -1$. Physical interpretation of this measurement is as follows: If the measured values (q, p) of the oscillator (yellow-shaded disks in Fig. 1) are included in the width of the coherent-state projector (blue-shaded disks in Fig. 1), we will obtain the measurement result $+1$; otherwise, the measurement result is -1 .

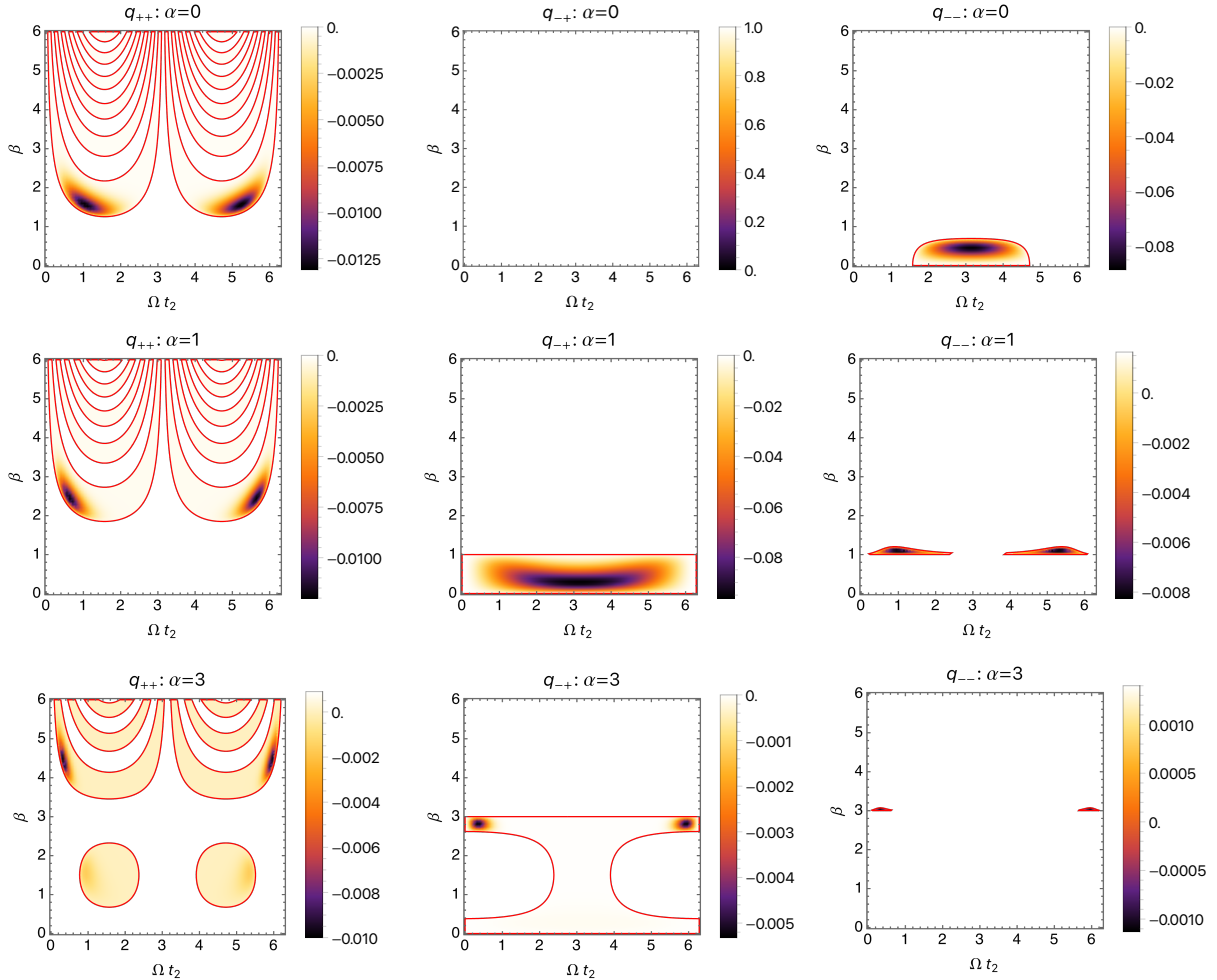


FIG. 2. Negative regions of the quasi-probability (enclosed by red lines) for the pure state $|\alpha\rangle$ with $\alpha = 0, 1$, and 3 . For $\alpha = 0$, q_{++} and q_{--} become negative. For $\alpha \neq 0$, q_{++} , q_{--} , and q_{-+} become negative. We chose $t_1 = 0$ and $\omega = \Omega$.

C. Quasi-probability with a coherent-state projector for the initial thermal coherent state

By using the measurement operator (21), the quasi-probability with an initial thermal coherent state (12) becomes

$$\begin{aligned} q_{s_1 s_2} &= C \text{ReTr} \left[\hat{M}_{s_2}(t_2) \hat{M}_{s_1}(t_1) \hat{D}(\alpha) e^{-A\hat{a}^\dagger \hat{a}} \hat{D}^\dagger(\alpha) \right] \\ &= C \text{ReTr} \left[\hat{D}^\dagger(\alpha) \hat{M}_{s_2}(t_2) \hat{D}(\alpha) \hat{D}^\dagger(\alpha) \hat{M}_{s_1}(t_1) \hat{D}(\alpha) e^{-A\hat{a}^\dagger \hat{a}} \right], \end{aligned} \quad (22)$$

where

$$\hat{D}^\dagger(\alpha) \hat{M}_s(t) \hat{D}(\alpha) = \frac{1-s}{2} + s |\gamma(t) - \alpha, \zeta(t)\rangle \langle \gamma(t) - \alpha, \zeta(t)|. \quad (23)$$

Then, using $e^{-A\hat{a}^\dagger \hat{a}} = \sum_n e^{-A n} |n\rangle \langle n|$ in Eq. (22) gives

$$\begin{aligned} q_{s_1 s_2} &= C \text{Re} \sum_n \left[\frac{(1-s_1)(1-s_2)}{4} e^{-A n} + \frac{s_1(1-s_2)}{2} e^{-A n} |\langle n | \gamma_1 - \alpha, \zeta_1 \rangle|^2 \right. \\ &\quad + \frac{s_2(1-s_1)}{2} e^{-A n} |\langle n | \gamma_2 - \alpha, \zeta_2 \rangle|^2 \\ &\quad \left. + s_1 s_2 e^{-A n} \langle \gamma_2 - \alpha, \zeta_2 | \gamma_1 - \alpha, \zeta_1 \rangle \langle n | \gamma_2 - \alpha, \zeta_2 \rangle \langle \gamma_1 - \alpha, \zeta_1 | n \rangle \right]. \end{aligned} \quad (24)$$

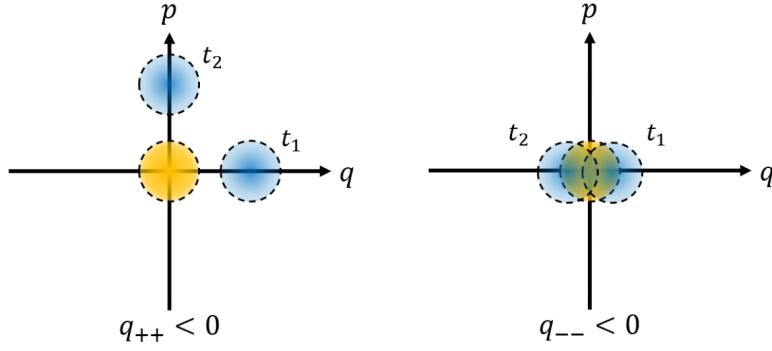


FIG. 3. Schematic explanation of violation of the LGIs for the coherent-state projector. Yellow regions represent the initial state of the oscillator, and blue regions represent 1σ contours of the projector. The left panel represents the projector with $\beta > 1$ and the right panel represents the projector with $\beta < 1$.

For a coherent-state projector without squeezing, we set $\zeta = 0$ and $\gamma = \beta$ and the quasi-probability is evaluated as

$$\begin{aligned}
q_{s_1 s_2} &= C \operatorname{Re} \left[\frac{(1-s_1)(1-s_2)}{4} \sum_n e^{-A n} \right. \\
&\quad + \frac{s_1(1-s_2)}{2} e^{-|\beta_1-\alpha|^2} \sum_n e^{-A n} \frac{|\beta_1-\alpha|^{2n}}{n!} + \frac{s_2(1-s_1)}{2} e^{-|\beta_2-\alpha|^2} \sum_n e^{-A n} \frac{|\beta_2-\alpha|^{2n}}{n!} \\
&\quad \left. + s_1 s_2 \langle \beta_2 - \alpha | \beta_1 - \alpha \rangle e^{-|\beta_2-\alpha|^2/2 - |\beta_1-\alpha|^2/2} \sum_n e^{-A n} \frac{(\beta_2 - \alpha)^n (\beta_1^* - \alpha^*)^n}{n!} \right] \\
&= C \operatorname{Re} \left[\frac{(1-s_1)(1-s_2)}{4} \frac{1}{1 - e^{-A}} \right. \\
&\quad + \frac{s_1(1-s_2)}{2} e^{-|\beta_1-\alpha|^2} \exp(e^{-A} |\beta_1 - \alpha|^2) + \frac{s_2(1-s_1)}{2} e^{-|\beta_2-\alpha|^2} \exp(e^{-A} |\beta_2 - \alpha|^2) \\
&\quad \left. + s_1 s_2 e^{-|\beta_2-\alpha|^2 - |\beta_1-\alpha|^2} e^{(\beta_2^* - \alpha^*)(\beta_1 - \alpha)} \exp(e^{-A} (\beta_2 - \alpha)(\beta_1^* - \alpha^*)) \right] \\
&= \frac{(1-s_1)(1-s_2)}{4} + (1 - e^{-A}) \left[\frac{s_1(1-s_2)}{2} e^{-|\beta_1-\alpha|^2} \exp(e^{-A} |\beta_1 - \alpha|^2) \right. \\
&\quad + \frac{s_2(1-s_1)}{2} e^{-|\beta_2-\alpha|^2} \exp(e^{-A} |\beta_2 - \alpha|^2) \\
&\quad \left. + s_1 s_2 e^{-|\beta_2-\alpha|^2 - |\beta_1-\alpha|^2} \operatorname{Re} e^{(\beta_2^* - \alpha^*)(\beta_1 - \alpha)} \exp(e^{-A} (\beta_2 - \alpha)(\beta_1^* - \alpha^*)) \right], \tag{25}
\end{aligned}$$

where $\beta_1 := e^{i\Omega t_1} \beta$ and $\beta_2 := e^{i\Omega t_2} \beta$. For the zero-temperature limit $e^{-A} \rightarrow 0$,

$$\begin{aligned}
q_{s_1 s_2} &= \frac{(1-s_1)(1-s_2)}{4} + \frac{s_1(1-s_2)}{2} e^{-|\beta_1-\alpha|^2} + \frac{s_2(1-s_1)}{2} e^{-|\beta_2-\alpha|^2} \\
&\quad + s_1 s_2 e^{-|\beta_2-\alpha|^2 - |\beta_1-\alpha|^2} \operatorname{Re} e^{(\beta_2^* - \alpha^*)(\beta_1 - \alpha)}. \tag{26}
\end{aligned}$$

Furthermore, for the vacuum state $\alpha = 0$, the quasi-probability $q_{s_1 s_2}$ depends only on the difference between the two measurement times $\Omega(t_2 - t_1)$ and β . For the high-temperature limit $e^{-A} \rightarrow 1$, the quasi-probability becomes $q_{s_1 s_2} = (1-s_1)(1-s_2)/4 \geq 0$ and the LGIs are not violated within this limit.

The features and interpretation of violation of the LGIs for the initial vacuum state, initial coherent state, and initial thermal state are as follows:

a. *Initial vacuum state $\alpha = 0$:* The first row in Fig. 2 shows the behaviour of the quasi-probability with an initial vacuum state $|0\rangle$ (Eq. (26)), where we chose $t_1 = 0$ and $\omega = \Omega$. Regions where $q_{s_1 s_2} < 0$ (enclosed by red lines) is in the (t, β) plane. Figure 3 shows a schematic interpretation of the violation of the LGIs with a coherent projector. In this case, q_{++} and q_{--} are negative. For a projector with parameter $\beta < 1$, because the target vacuum state of the oscillator is localized at $q \sim 0$, the measurement discriminates whether the particle is located around $q \sim 0$ (measurement with $s = +1$) or not (measurement result with $s = -1$). Hence, q_{++} does not violate the LGIs with

this value of the parameter β ; Immediately after the first measurement, the particle is definitely located around $q \sim 0$ and the second measurement will result in the same result as the first measurement, and these measurement results are classically expected. However, q_{--} represents the “possibility” that a particle does not exist around $q = 0$ for both the first and second measurements, and such a measurement result cannot be expected classically. Therefore, q_{--} becomes negative and MR is violated. Furthermore, it can be expected that the maximum violation occurs at the half period $\Omega t_2 = \pi$ because of the largest overlap between the yellow region (state of the oscillator) and blue region (projector) in the right panel of Fig. 3. For the $\beta = 0$ case, $q_{s_1 s_2} = (1 + s_1)(1 + s_2)/4 \geq 0$ and there is no violation of the LGIs. This is because the measurement with $\beta = 0$ does not disturb the target vacuum state, and the obtained measurement results coincide with the classical results (and the particle always exists at $q = 0$ in this case). For $\beta > 1$, q_{++} is negative. Negative regions in q_{++} form a fringe structure that implies quantum interference of the oscillator motion; indeed, the quasi-probability for the initial vacuum state is regarded as overlap of two branches of evolved states $|\psi_1\rangle := \hat{M}_+(t_1)|0\rangle$ and $|\psi_2\rangle := \hat{M}_+(t_2)|0\rangle$, and $\langle\psi_1|\psi_2\rangle$ represents interference of these two branches. After the first measurement at t_1 , the center of the wavefunction is projected to the location where $\beta > 1$ and then evolves according to the classical equation of motion. Because classical particle motion is oscillatory in time, the measurement result $Q_{s_1=1} = Q_{s_2=1} = +1$ cannot be expected classically. The measurement result depends on the value of $t_2 - t_1$. Therefore, q_{++} was negative.

b. *Initial coherent state $\alpha \neq 0$:* The second and third rows in Fig. 2 show the behaviour of the quasi-probability with an initial coherent state $|\alpha\rangle$ (Eq. (26)), where we chose $t_1 = 0$ and $\omega = \Omega$. Regions where $q_{s_1 s_2} < 0$ (enclosed by red lines) are in the (t, β) plane. In this case, q_{++} , q_{-+} , and q_{--} are negative. We can provide the following explanation for the emergence of negative regions in the quasi-probability: q_{++} exhibits a fringe pattern in the region $\beta > \alpha$, which is the same behavior as that in the $\alpha = 0$ case. Because the quasi-probability with the initial coherent state overlaps the two states $\hat{M}(t_1)|\alpha\rangle$ and $\hat{M}(t_2)|\alpha\rangle$, it represents interference between these two states. For $\beta > \alpha$, the interference fringe appears as a negative value for q_{++} in the (t, β) plane. If we focus only on the position of the oscillator, where the value of the violation is relatively large (dark black region in Fig. 2), then we observe that the relation $\beta \sim \alpha \pm 1.5$ (> 1) holds with any α . This relationship explains why round regions with a negative quasi-probability suddenly appear in the lower left panel of Fig. 2. Although not included in the figure, as can be seen from the relation $\beta \sim \alpha \pm 1.5$, round regions with negative quasi-probabilities begin to appear when α begins to exceed ~ 2.5 . Physically, one could say that an overlap between the state of the oscillator and the projector that is neither too large nor too small is required for a violation of the LGIs (Fig. 3). For q_{-+} , if we select the $\alpha = 1$ case as shown in Fig. 4, the first measurement result implies that the particle exists around the yellow region ($Q = -1$), but the second measurement confirms that the particle exists around the green region ($Q = +1$), which is not classically expected. Of course, we must consider the spread of the oscillator’s wavefunction; this effect is omitted here for intuitive understanding. The quasi-probability q_{--} can become negative in narrow regions with $\alpha \sim \beta$ in the (t, β) plane. That the first and second measurement results predict the nonexistence of the particle around $q = 0$ is not classically expected because the yellow region (state of the oscillator) and blue regions (projector) overlap (Fig. 3). Therefore, q_{--} has negative values and the LGIs are violated.

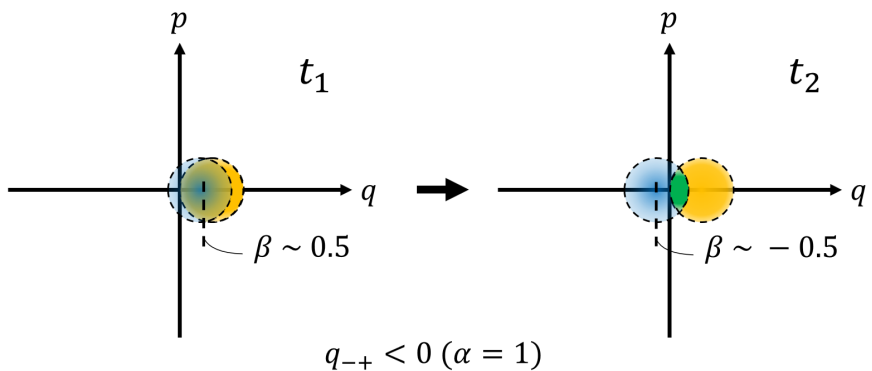


FIG. 4. Schematic explanation of violation of the LGIs for q_{-+} with $\alpha = 1$ and $\beta \sim 0.5$. At time $t = t_1$, $s_1 = -1$, and the particle is expected to be in the yellow region. Then, at time $t = t_2$, the particle is expected to be in the green region because $s_2 = +1$. The mismatch in location in the phase space between the yellow region on the left panel ($t = t_1$) and the green region on the right panel ($t = t_2$) leads to the violation of the LGIs.

c. *Initial thermal state:* Figure 5 shows the thermal effect on the negativity of the quasi-probability. For the initial mixed states with $\nu = 0.51, 0.61, and 0.75 , the negative regions of $q_{s_1 s_2}$ become smaller with an increase in ν compared with those of the initial vacuum state. Therefore, the thermal effect (mixedness of the initial states) reduces violation of the LGIs. Above the critical value of ν , violation of the LGIs is not observed in q_{--} . Figure 6 shows the time dependence of q_{++} (with $\beta = 1.6$) and q_{--} (with $\beta = 0.5$) for $\nu = 0.5, 0.61, and 0.75 . This shows that the smallest negative values of the quasi-probability approach zero with an increase in ν and the thermal effect prevents violation of the LGIs.$$

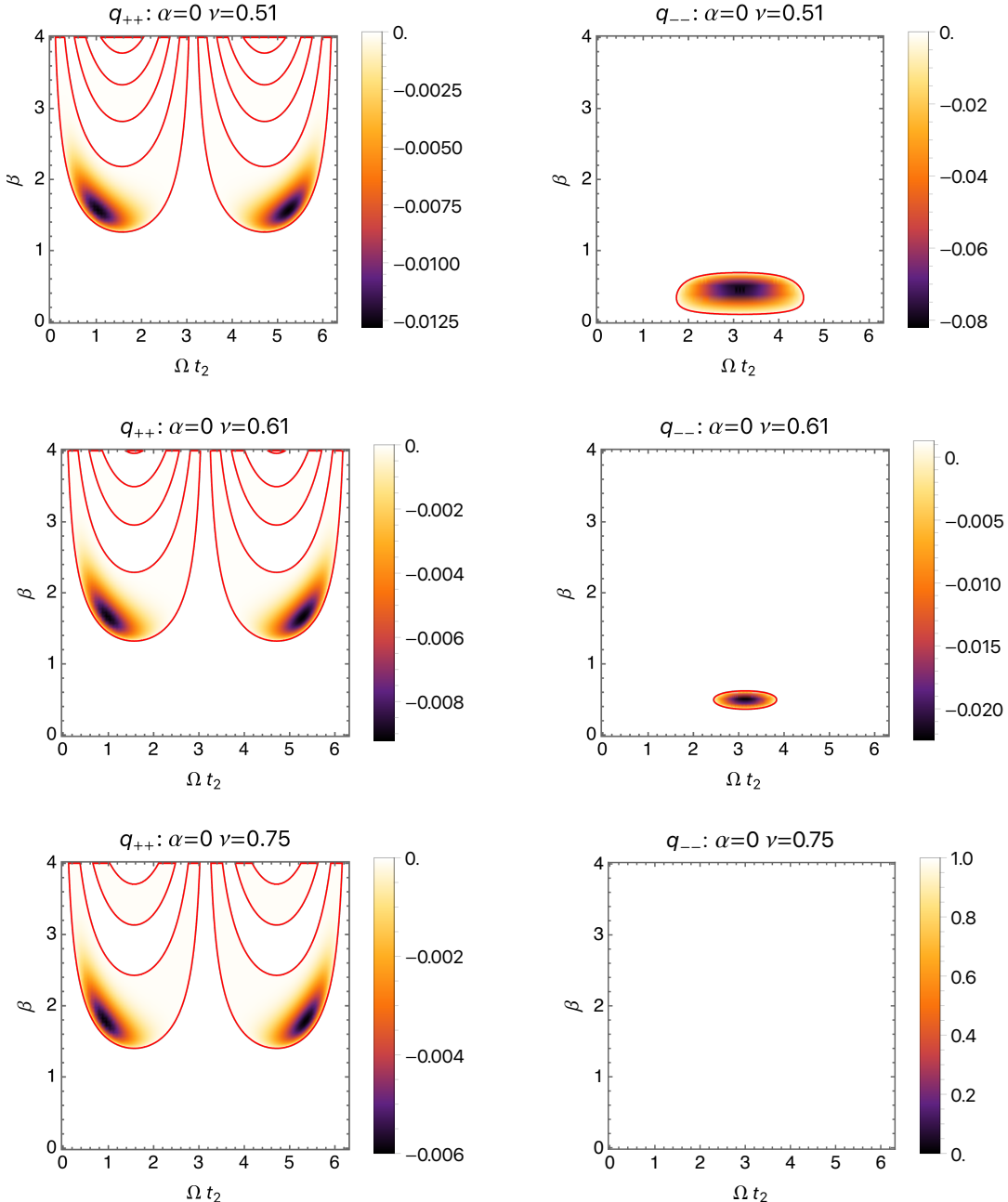


FIG. 5. Negative regions of the quasi-probability (enclosed by red lines) for the initial thermal state $\alpha = 0$ with $\nu = 0.51, 0.61$, and 0.75 . $\nu = 0.5$ corresponds to a pure state. As ν increases, the thermal effect reduces the violation of the LGIs. We chose $t_1 = 0$ and $\omega = \Omega$.

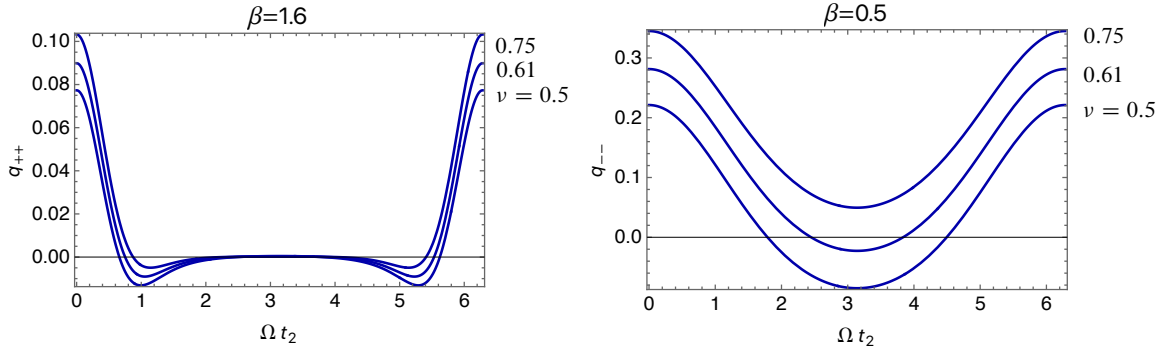


FIG. 6. Time dependence of the quasi-probability q_{++} with $\beta = 1.6$ (left panel) and q_{--} with $\beta = 0.5$ (right panel) for the initial thermal state with $\nu = 0.5, 0.61$, and 0.75 . $\nu = 0.5$ corresponds to a pure state. The thermal effect reduces violation of the LGIs. For $\nu = 0.75$, q_{--} does not have negative values.

D. Quasi-probability with a squeezed coherent-state projector in the initial vacuum state

Now, we consider a projector with a squeezed coherent state (21) for the initial vacuum state. After taking the zero-temperature limit $A \rightarrow \infty$ and $\alpha = 0$ in Eq. (22), the quasi-probability with the initial vacuum state is

$$q_{s_1 s_2} = \text{Re} \left[\frac{(1-s_1)(1-s_2)}{4} + \frac{s_1(1-s_2)}{2} |\langle 0 | \gamma_1, \zeta_1 \rangle|^2 + \frac{s_2(1-s_1)}{2} |\langle 0 | \gamma_2, \zeta_2 \rangle|^2 + s_1 s_2 \langle \gamma_2, \zeta_2 | \gamma_1, \zeta_1 \rangle \langle 0 | \gamma_2, \zeta_2 \rangle \langle \gamma_1, \zeta_1 | 0 \rangle \right], \quad (27)$$

where²

$$\langle 0 | \gamma_j, \zeta_j \rangle = \frac{1}{\sqrt{\cosh r}} \exp \left[-\frac{\gamma^2}{2} (1 + \tanh r) \right]. \quad (28)$$

has no time dependence. Therefore, the quasi-probability is given by

$$q_{s_1 s_2} = \frac{(1-s_1)(1-s_2)}{4} + |\langle 0 | \gamma, \zeta \rangle|^2 \left[\frac{s_1(1-s_2)}{2} + \frac{s_2(1-s_1)}{2} + s_1 s_2 \text{Re} \langle \gamma_2, \zeta_2 | \gamma_1, \zeta_1 \rangle \right], \quad (29)$$

with

$$\langle \gamma_2, \zeta_2 | \gamma_1, \zeta_1 \rangle = \frac{1}{\sqrt{\sigma_{21}}} \exp \left[\frac{\eta_{21} \eta_{12}^*}{2\sigma_{21}} + \frac{1}{2} (\gamma_2 \gamma_1^* - \gamma_2^* \gamma_1) \right], \quad (30)$$

$$\sigma_{21} = \cosh^2 r - e^{2i\Omega(t_2-t_1)} \sinh^2 r, \quad (31)$$

$$\eta_{21} = (e^{i\Omega t_2} - e^{i\Omega t_1}) \gamma \cosh r - (e^{-i\Omega t_2} - e^{-i\Omega t_1}) \gamma e^{i(2\Omega t_2 + \pi)} \sinh r, \quad (32)$$

$$\eta_{12} = -(e^{i\Omega t_2} - e^{i\Omega t_1}) \gamma \cosh r + (e^{-i\Omega t_2} - e^{-i\Omega t_1}) \gamma e^{i(2\Omega t_1 + \pi)} \sinh r, \quad (33)$$

$$\gamma_2 \gamma_1^* = e^{i\Omega(t_2-t_1)} \gamma^2, \quad (34)$$

$$\eta_{21} \eta_{12}^* = \gamma^2 e^{-i\Omega(t_2-t_1)} (1 - e^{i\Omega(t_2-t_1)})^2 (\cosh r - e^{i\Omega(t_2-t_1)} \sinh r)^2, \quad (35)$$

$$\gamma_2 \gamma_1^* - \gamma_2^* \gamma_1 = (e^{i\Omega(t_2-t_1)} - e^{-i\Omega(t_2-t_1)}) \gamma^2. \quad (36)$$

² We use the following formulas for the squeezed coherent state $|\beta, \xi\rangle$, where $\xi = e^{i\varphi} r$ [18]:

$$\langle 0 | \beta, \xi \rangle = \frac{1}{\sqrt{\cosh r}} \exp \left[-\frac{1}{2} |\beta|^2 + \frac{e^{i\varphi}}{2} \beta^{*2} \tanh r \right],$$

$$\langle \beta_1, \xi_1 | \beta_2, \xi_2 \rangle = \frac{1}{\sqrt{\sigma_{21}}} \exp \left[\frac{\eta_{21} \eta_{12}^*}{2\sigma_{21}} + \frac{1}{2} (\beta_2 \beta_1^* - \beta_2^* \beta_1) \right],$$

for $r_2 = r_1 \equiv r$, where

$$\sigma_{21} = \cosh^2 r - e^{i(\varphi_2 - \varphi_1)} \sinh^2 r,$$

$$\eta_{21} = (\beta_2 - \beta_1) \cosh r - (\beta_2^* - \beta_1^*) e^{i\varphi_2} \sinh r, \quad \eta_{12} = (\beta_1 - \beta_2) \cosh r - (\beta_1^* - \beta_2^*) e^{i\varphi_1} \sinh r$$

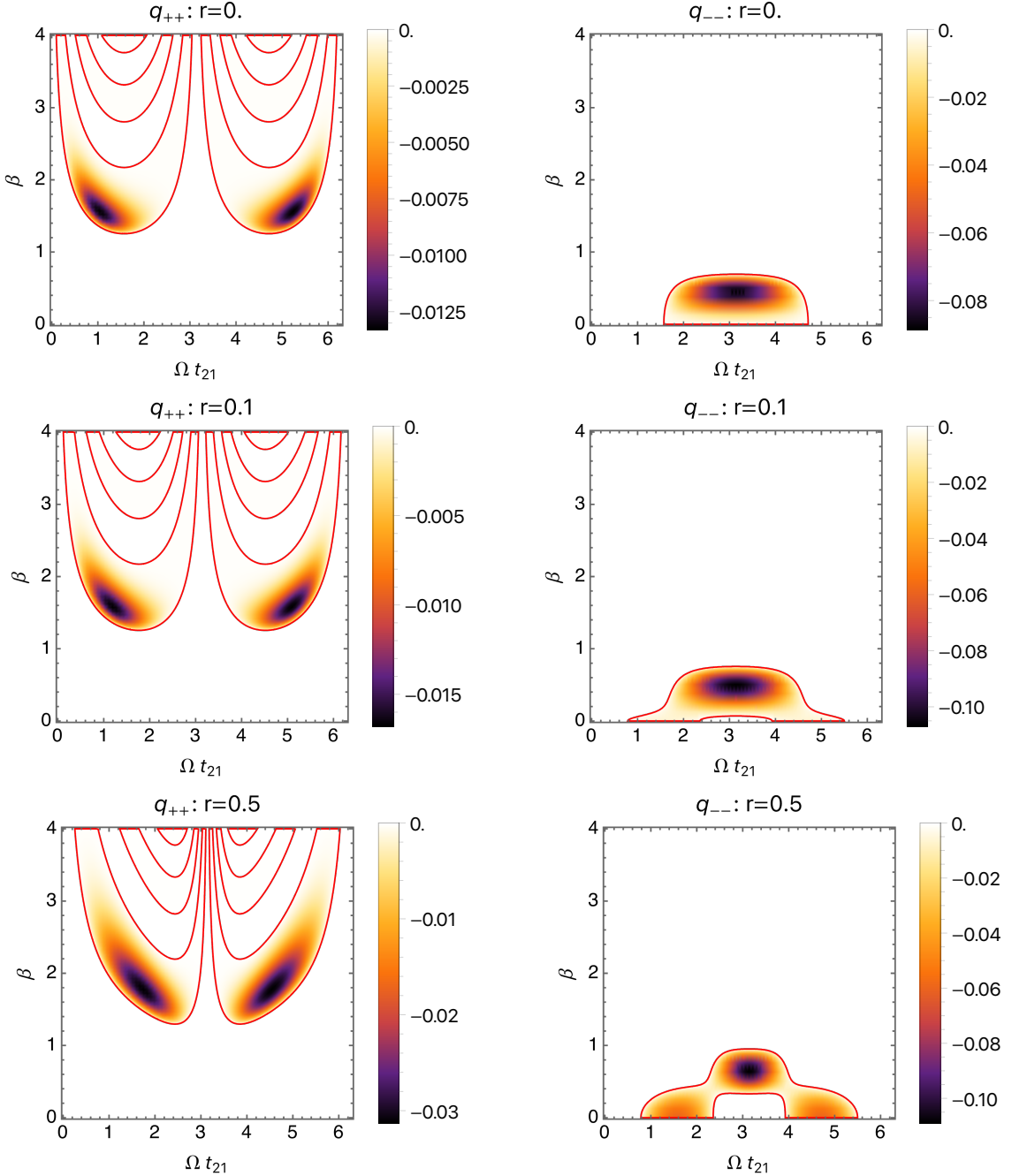


FIG. 7. Negative regions of the quasi-probability (enclosed by red lines) for the pure ground state $|0\rangle$ with the squeezed coherent-state projector $r > 0$. q_{++} and q_{--} have negative values and the LGIs are violated.

The time dependence of $q_{s_1 s_2}$ was determined as a function of the time difference $t_{21} = t_2 - t_1$.

Figures 7 and 8 show the negative regions of the quasi-probability for the vacuum state with a squeezed coherent-state projector. The structures of the negative regions in q_{++} and q_{--} are essentially identical to those in the coherent-state-projector case. However, the squeezing effect of the projector affects the shapes of the negative regions of the quasi-probability and their negative values.

First, we consider the $r > 0$ case (Figs. 7 and 9). We observe that squeezing with $r > 0$ enhances the violation of the LGIs in q_{--} (see Fig. 9, which depicts (r, β) dependence of q_{--} at $\Omega t_{21} = \pi$). In fact, when $r \approx 0.31$, q_{--} can reach ~ -0.123 at $\beta \approx 0.57, \Omega t_{21} = \pi$, which is close to the value of the Lüders bound $-1/8 = -0.125$, and a nearly maximal violation of the LGIs is realized. The maximum violation setting of the LGIs is similar to that for q_{--} with

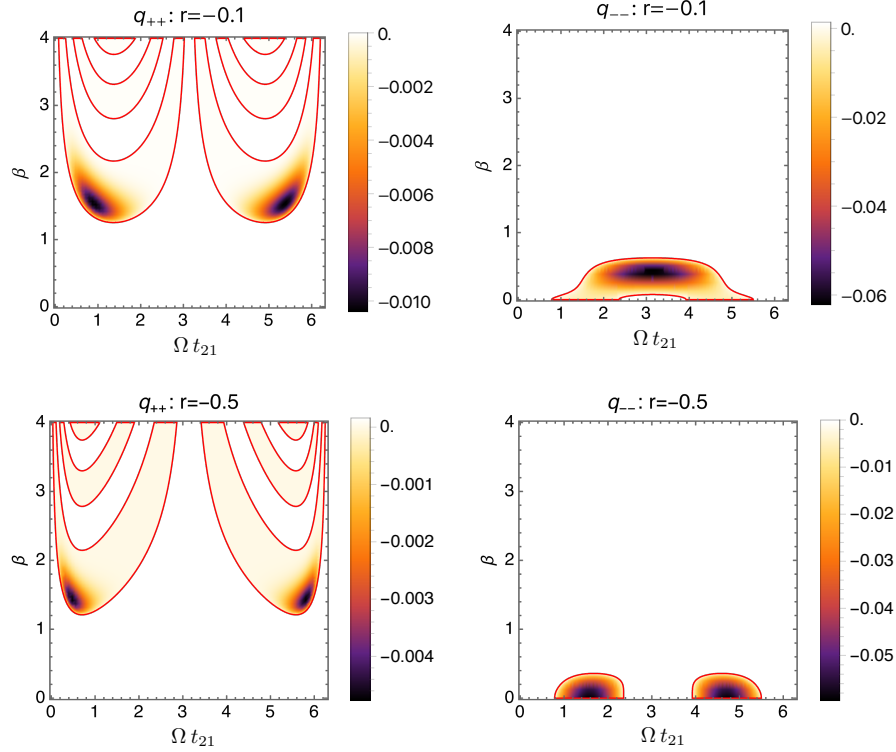


FIG. 8. Negative regions of the quasi-probability (enclosed by red lines) for the pure ground state $|0\rangle$ with squeezed coherent-state projector $r < 0$. q_{++} and q_{--} have negative values and the LGIs are violated.

a coherent-state projector for the initial vacuum state (see q_{--} ($\alpha = 0$) in Fig. 2) but, in terms of the amount of violation, it becomes greater with the introduction of the squeezing. This reflects the fact that the squeezed state itself represents a quantum nature compared with the simple coherent state without squeezing. For q_{++} , its values decrease with the increase in r . Therefore, squeezing enhances the violations of the LGIs that appears in q_{++} .

Figure 10 shows a schematic explanation of the violation of the LGIs by a squeezed coherent-state projector. This figure helps us understand why quasi-probability is negative in some of the panels of Fig. 8. Figure 11 conversely illustrates typical examples of a setting in which quasi-probability is not negative (i.e., the LGIs are not violated). The left panel explains why the quasi-probability is not negative in the half period ($\Omega t_{21} = \pi$) for the lower right panel in Fig. 8. That is, in the orange region, where the particles are predicted to be present, the second measurement measures almost the same region as the first measurement; therefore, we can say that no information is obtained from the second measurement.

For the $r < 0$ case (Figs. 8 and 9), we observe that the squeezing increases negative values of q_{++} and q_{--} and reduces violation of the LGIs. Therefore, squeezing did not enhance the violation of the LGIs in this case. As r decreases (e.g., $r = -0.5$), the position of the maximum violation changes from $\Omega t_{21} = \pi$ (a half period) to $\Omega t_{21} = \pi/2$ (a quarter period) and $\Omega t_{21} = 3\pi/2$ (a three-quarter period). As shown in the schematic explanation of the violation of the LGIs (left panel of Fig. 11), this corresponds to the fact that, at $\Omega t_{21} = \pi$, we perform the measurement for almost the same area as measured at t_1 . Therefore, we did not obtain any information and the LGIs were not violated.

For larger absolute values of the squeezing parameter $|r| \gg 1$, the negative value of the quasi-probability approaches zero for q_{++} . This can be explained as follows: A projector with these values of r corresponds to an ideal projective q or p measurement (see the middle and right panels of Fig. 11). These types of measurements project the target state onto the position eigenstate or momentum eigenstate after the measurement. In other words, if $|r|$ is large, the state of the particle collapses to the position or momentum eigenstate, and a violation of the LGIs is not expected. For q_{--} , the state is projected to the outside of the blue region, as shown in Fig. 11. When $|r| \gg 1$, the projected region is almost the same as the original vacuum state, which gives results that are not significantly different from classical motion. This indicates that the information obtained from this measurement was insufficient. We observe a similar feature of suppressing the violation of the LGIs for a quantum field with a local projection operator with a large squeezing parameter.

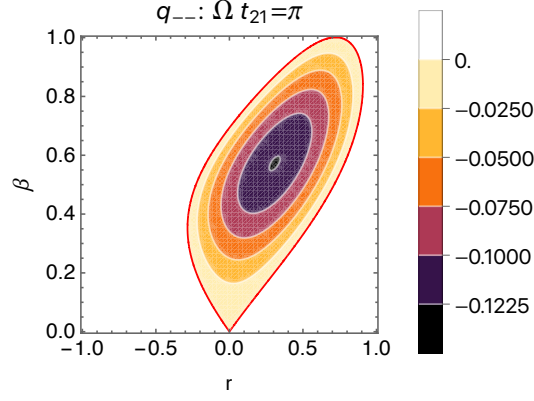


FIG. 9. Dependence of (r, β) for negative values of q_{--} at $\Omega t_{21} = \pi$. At $(r, \beta) \sim (0.31, 0.57)$, the maximum violation of the LGIs close to the Lüders bound is realized.

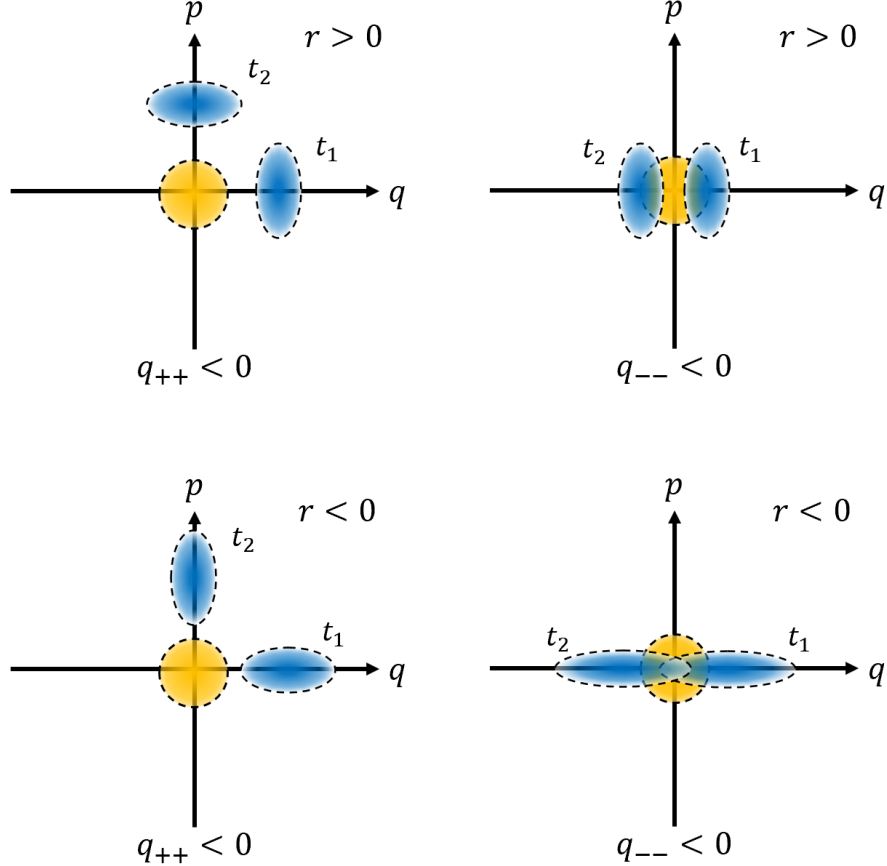


FIG. 10. Schematic explanation of the LGIs violation with the squeezed coherent-state projector. The distribution of particles and projectors when the squeezing parameter r is positive is shown in the upper panel, and that when r is negative is shown in the lower panel. q_{++} is the left panel, and q_{--} is the right panel. The deviation of the projector (blue region) from the origin is the coherent amplitude β . Therefore, we can see that, in q_{--} , LGIs violation is occurring between $\beta = 0$ and $\beta = 1$ even when the projector is squeezed.

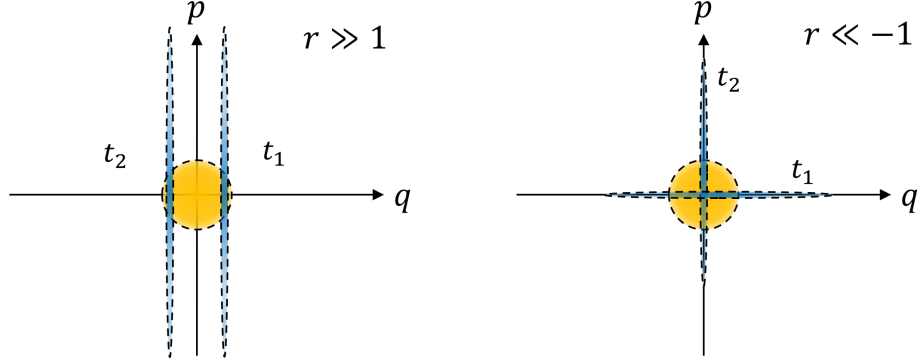


FIG. 11. Typical examples of $q_{--} > 0$. The left and right panels represent the extreme case of squeezing, in which the LGIs are not violated. For large $|r|$, the state after measurement becomes approximately eigenstates of \hat{q} or \hat{p} , and the violation of the LGIs cannot be expected.

III. VIOLATION OF LGIS FOR A QUANTUM FIELD

As an application of the coherent-state projector, we investigated LGIs for a chiral scalar field that appears as an edge excitation of quantum-Hall systems [19]. To formulate the LGIs for the quantum field, we first introduce the spatial local modes of the quantum field.

A. Chiral scalar field in $(1+1)$ -dimensional spacetime

We consider a quantum chiral scalar field $\hat{\varphi}$ corresponding to the edge excitation of a quantum Hall system [20, 21]. Our main purpose is to investigate the quantum effect of edge modes in a quantum Hall system, which is measurable using the local charge density $\partial_x \hat{\varphi}$. The scalar field obeys the following $(1+1)$ -dimensional Klein–Gordon equation:

$$\ddot{\hat{\varphi}} - v^2 \partial_x^2 \hat{\varphi} = 0, \quad (37)$$

where v is the propagation speed of edge excitation. It is determined as

$$v = \frac{cU'(y)}{eB} = \frac{cE}{B}, \quad (38)$$

where $U(y)$ is the trapping potential perpendicular to the edges of the quantum Hall system, E is the electric field induced by U , and B is the perpendicular magnetic field. Hereafter, we set $v = 1$ and adopt v as the units of length and time.

The field operator at $x^+ = t + x$ is expressed as

$$\hat{\varphi}(x^+) = \int_0^\infty \frac{dk}{\sqrt{4\pi k}} \left[\hat{a}_k e^{-ikx^+} + \hat{a}_k^\dagger e^{ikx^+} \right]. \quad (39)$$

We assumed a vacuum state in the quantum field by imposing $\hat{a}_k |g\rangle = 0$. In our setup, the gauge-invariant physical quantity is the current (charge) density given by the derivative of the field operator $\hat{\varphi}$:

$$\hat{\Pi}(x^+) := \hat{\varphi}'(x^+) = -i \int_0^\infty dk \sqrt{\frac{k}{4\pi}} \left[\hat{a}_k e^{-ikx^+} - \hat{a}_k^\dagger e^{ikx^+} \right]. \quad (40)$$

The commutators between the field operators are

$$[\hat{\varphi}(x^+), \hat{\varphi}(y^+)] = -\frac{i}{4} \text{sgn}(x^+ - y^+), \quad (41)$$

$$[\hat{\varphi}(x^+), \hat{\Pi}(y^+)] = \frac{i}{2} \delta(x^+ - y^+), \quad (42)$$

$$[\hat{\Pi}(x^+), \hat{\Pi}(y^+)] = \frac{i}{2} \delta'(x^+ - y^+). \quad (43)$$

The two-point correlation functions areas are as follows:

$$\langle \{\hat{\varphi}(x^+), \hat{\varphi}(y^+)\} \rangle = \frac{1}{2\pi} \int_0^\infty \frac{dk}{k} \cos(k(x^+ - y^+)), \quad (44)$$

$$\langle \{\hat{\varphi}(x^+), \hat{\Pi}(y^+)\} \rangle = \frac{1}{2\pi} \int_0^\infty dk \sin(k(x^+ - y^+)), \quad (45)$$

$$\langle \{\hat{\Pi}(x^+), \hat{\Pi}(y^+)\} \rangle = \frac{1}{2\pi} \int_0^\infty dk k \cos(k(x^+ - y^+)). \quad (46)$$

The Wightman function for $\hat{\varphi}$ is

$$\begin{aligned} D_\varphi(x_1^+, x_2^+) &= \langle \hat{\varphi}(x_1^+) \hat{\varphi}(x_2^+) \rangle = \frac{1}{4\pi} \int_\mu^\infty \frac{dk}{k} e^{-ik(x_1^+ - x_2^+ - i\epsilon)}, \\ &= -\frac{1}{4\pi} \log[\mu(x_1^+ - x_2^+ - i\epsilon)], \end{aligned} \quad (47)$$

where we introduce an IR cutoff μ as the lower bound of the integral and a UV cutoff ϵ by $\epsilon := \Delta x$, where Δx is the spatial cutoff length. In our analysis, the chiral scalar field $\hat{\varphi}$ is an effective one and there exists a short cutoff length ϵ , below which the effective treatment of the edge mode breaks down. In a quantum Hall system, this scale is given by the magnetic length of the quantum Hall system:

$$\ell_B = \sqrt{\frac{\hbar}{eB}}. \quad (48)$$

We considered the short-length cutoff Δx as the length in our analysis. The Wightman function for $\hat{\Pi}$ is as follows:

$$\begin{aligned} D_\Pi(x_1^+, x_2^+) &:= \langle \hat{\Pi}(x_1^+) \hat{\Pi}(x_2^+) \rangle = \partial_{x_1^+} \partial_{x_2^+} D(x_1^+, x_2^+) \\ &= \frac{1}{4\pi} \int_0^\infty dk k \left[e^{-ik(x_1^+ - x_2^+ - i\epsilon)} \right] \\ &= -\frac{1}{4\pi} \frac{1}{(x_1^+ - x_2^+ - i\epsilon)^2}. \end{aligned} \quad (49)$$

This quantity exhibits the same behavior as that of the massless scalar field in four-dimensional spacetime and is independent of the IR cutoff μ .

B. Local spatial modes of a quantum field

We considered measurements of the current density $\hat{\Pi}(x^+)$ at point x_A . The measurement can be represented by the following interaction Hamiltonian between $\hat{\Pi}$ and the canonical variables of the measurement apparatus (\hat{q}_D, \hat{p}_D) :

$$\hat{H}_{\text{int}} = \lambda(t) g(\hat{q}_D, \hat{p}_D) \otimes \int dx w_A(x) \hat{\Pi}(t + x), \quad (50)$$

where $g(\hat{q}_D, \hat{p}_D)$ is a function of the canonical variables of the measurement apparatus, $w_A(x)$ is a window function that defines the spatial mode of the field at x_A , and $\lambda(t)$ is a switching function. After acting on the apparatus,

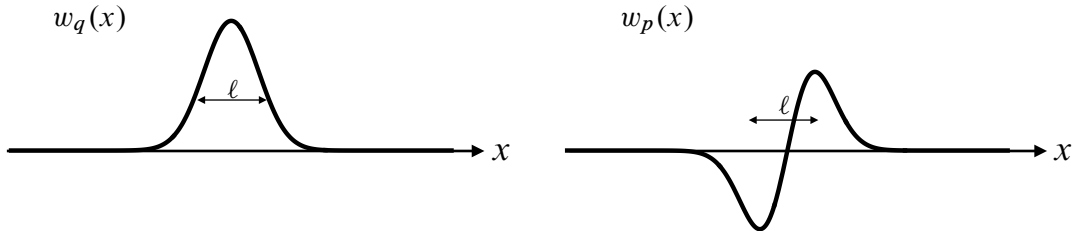


FIG. 12. Spatial profiles of window functions $w_q(x)$ and $w_p(x)$.

interaction causes a change in the “reading” of the apparatus depending on the state of the quantum field $\hat{\Pi}$ at x_A . In the present analysis, we did not introduce the details of the measurement protocols but only focused on the behavior of the local mode of the quantum field introduced by the spatial window function.

To measure the values of the field and its conjugate momentum, we define canonical variables corresponding to the local spatial modes of field at x_A as follows:

$$\hat{q}(t) = \int dx w_q(x - x_A) \hat{\Pi}(t + x), \quad \hat{p}(t) = \int dx w_p(x - x_A) \hat{\Pi}(t + x), \quad (51)$$

where $w_{p,q}(x)$ are window functions with nonzero values in a compact spatial region $x \in [-\ell/2, \ell/2]$. By requiring these operators to be canonical pairs, equal-time commutators between these operators should be

$$[\hat{q}, \hat{p}] = \frac{i}{2} \int dx w_q(x - x_A) w'_p(x - x_A) \equiv i, \quad (52)$$

$$[\hat{q}, \hat{q}] = \frac{i}{2} \int dx w_q(x - x_A) w'_q(x - x_A) \equiv 0, \quad (53)$$

$$[\hat{p}, \hat{p}] = \frac{i}{2} \int dx w_p(x - x_A) w'_p(x - x_A) \equiv 0. \quad (54)$$

These conditions are independent of the quantum field state. Hence, the local spatial mode (\hat{q}, \hat{p}) can be introduced as suitably choosing window functions $w_q(x)$ and $w_p(x)$ irrespective of the states of the quantum field. Locality of the spatial mode is guaranteed if window functions are adopted in which support is compact. We chose the following p -window function in our analysis:

$$w_p(x) = -w'_q(x), \quad \int dx (w'_q(x))^2 = 2, \quad (55)$$

and we assumed that the q -window function has the Gaussian form

$$w_q(x) = 2 \left(\frac{\ell^2}{\pi} \right)^{1/4} \exp \left(-\frac{x^2}{2\ell^2} \right). \quad (56)$$

The covariances of the local spatial modes are

$$\langle \hat{q}^2 \rangle = \frac{1}{2} \int dx dy w_q(x - x_A) w_q(y - x_A) \left\langle \left\{ \hat{\Pi}(t + x), \hat{\Pi}(t + y) \right\} \right\rangle, \quad (57)$$

$$\langle \hat{p}^2 \rangle = \frac{1}{2} \int dx dy w_p(x - x_A) w_p(y - x_A) \left\langle \left\{ \hat{\Pi}(t + x), \hat{\Pi}(t + y) \right\} \right\rangle, \quad (58)$$

$$\langle \hat{q}\hat{p} + \hat{p}\hat{q} \rangle = \int dx dy w_q(x - x_A) w_p(y - x_A) \left\langle \left\{ \hat{\Pi}(t + x), \hat{\Pi}(t + y) \right\} \right\rangle = 0, \quad (59)$$

where

$$\left\langle \left\{ \hat{\Pi}(t + x), \hat{\Pi}(t + y) \right\} \right\rangle = \frac{1}{2\pi} \int_0^\infty dk k \cos(k(x - y)) e^{-\epsilon k}. \quad (60)$$

Therefore,

$$\langle \hat{q}^2 \rangle = \frac{\ell^3}{\pi^{3/2}} \int_0^\infty dk e^{-\epsilon k} k \left(\int_{-\infty}^\infty dz e^{-z^2/2} \cos(k\ell z) \right)^2 = \frac{\ell}{\pi^{1/2}} \left(1 - \frac{\pi^{1/2}}{2} \left(\frac{\epsilon}{\ell} \right) + O \left(\frac{\epsilon}{\ell} \right)^2 \right), \quad (61)$$

$$\langle \hat{p}^2 \rangle = \frac{\ell}{\pi^{3/2}} \int_0^\infty dk e^{-\epsilon k} k \left(\int_{-\infty}^\infty dz z e^{-z^2/2} \sin(k\ell z) \right)^2 = \frac{1}{\pi^{1/2}\ell} \left(1 - \frac{3\pi^{1/2}}{4} \left(\frac{\epsilon}{\ell} \right) + O \left(\frac{\epsilon}{\ell} \right)^2 \right). \quad (62)$$

As $\nu^2 = \langle \hat{q}^2 \rangle \langle \hat{p}^2 \rangle = 1/\pi - 5/(4\pi^{1/2})(\epsilon/\ell) + O(\epsilon/\ell)^2$, the state of the local mode is generally thermal (for a pure state, $\nu = 1/2$). The mixedness of local mode depends on the region size ℓ and reflects the entanglement behavior between the local region and its complement. With an increase in ℓ , the symplectic eigenvalue ν increases, and the entanglement between the local modes and their complement becomes greater. This behavior of entanglement of the local mode was discussed in our previous study on a chiral scalar field in a quantum Hall system [21].

C. Measurement of a quantum field

We considered coherent-state measurements of the quantum field. The target local mode at $x = x_A$ defined by the quantum field is given as (51). The local modes are expressed as follows:

$$\hat{q}(t) = -\frac{i}{\sqrt{2}} \int_0^\infty dk k^{1/2} w_q(k) \left(e^{-ik(t+x_A)} \hat{a}_k - e^{ik(t+x_A)} \hat{a}_k^\dagger \right), \quad (63)$$

$$\hat{p}(t) = -\frac{1}{\sqrt{2}} \int_0^\infty dk k^{3/2} w_q(k) \left(e^{-ik(t+x_A)} \hat{a}_k + e^{ik(t+x_A)} \hat{a}_k^\dagger \right), \quad (64)$$

where the Fourier component of the window function is introduced as

$$w_q(k) = \frac{1}{\sqrt{2\pi}} \int_{-\infty}^\infty dx w_q(x) e^{ikx}, \quad w_q(k) = w_q^*(k), \quad w_p(k) = ik w_q(k) \quad (65)$$

and, for the window function (56),

$$w_q(k) = 2 \left(\frac{\ell^6}{\pi} \right)^{1/4} e^{-\frac{\ell^2}{2} k^2}. \quad (66)$$

The annihilation operator for the local mode is introduced as follows:

$$\begin{aligned} \hat{b}(t) &:= \sqrt{\frac{\omega}{2}} \hat{q}(t) + \frac{i}{\sqrt{2\omega}} \hat{p}(t) \\ &= -\frac{i}{2} \int_0^\infty dk k w_q(k) \left[\left(\sqrt{\frac{\omega}{k}} + \sqrt{\frac{k}{\omega}} \right) e^{-ik(t+x_A)} \hat{a}_k - \left(\sqrt{\frac{\omega}{k}} - \sqrt{\frac{k}{\omega}} \right) e^{+ik(t+x_A)} \hat{a}_k^\dagger \right] \\ &= -i \int_0^\infty dk k w_q(k) (\cosh r_k \hat{a}_k(t) - \sinh r_k \hat{a}_k^\dagger(t)), \end{aligned} \quad (67)$$

where ω is a parameter characterizing the local mode (a parameter characterizing the projector related to the protocols of the measurement apparatus) and we introduced r_k and $\hat{a}_k(t)$ as

$$e^{r_k} = \sqrt{\frac{\omega}{k}}, \quad \hat{a}_k(t) = e^{-ik(t+x_A)} \hat{a}_k. \quad (68)$$

We consider the following Gaussian projector for the local mode at time t :

$$\hat{M}_s(t) = \frac{1-s}{2} + s \hat{D}_{b(t)}(\beta) \hat{\rho}_{b(t)} \hat{D}_{b(t)}^\dagger(\beta), \quad (69)$$

$$\hat{D}_{b(t)}(\beta) = e^{\beta \hat{b}^\dagger(t) - \beta^* \hat{b}(t)}, \quad \hat{\rho}_{b(t)} = |0_{b(t)}\rangle \langle 0_{b(t)}|, \quad (70)$$

where $s = \pm 1$ and $\hat{\rho}_{b(t)}$ represents the state of measurement apparatus for the local mode. We use the following formula that connects the displacement operator to the vacuum density operator:

$$|0_{b(t)}\rangle \langle 0_{b(t)}| = \int \frac{d^2 z}{\pi} \exp \left[-\frac{1}{2} |z|^2 \right] \hat{D}_{b(t)}(z). \quad (71)$$

The Gaussian projector can then be written as³

$$\begin{aligned} \hat{M}_s(t) &= \frac{1-s}{2} + \frac{s}{\pi} \int d^2 z \exp \left[-\frac{1}{2} |z|^2 \right] \hat{D}_{b(t)}(\beta) \hat{D}_{b(t)}(z) \hat{D}_{b(t)}^\dagger(\beta) \\ &= \frac{1-s}{2} + \frac{s}{\pi} \int d^2 z \exp \left[-\frac{1}{2} |z|^2 \right] e^{-\beta^* z + \beta z^*} \hat{D}_{b(t)}(z). \end{aligned} \quad (72)$$

³ The formulas for the displacement operators are

$$\hat{D}(\lambda_1) \hat{D}(\lambda_2) = \hat{D}(\lambda_1 + \lambda_2) \exp \left\{ \frac{1}{2} (\lambda_1 \lambda_2^* - \lambda_1^* \lambda_2) \right\}, \quad \hat{D}(\lambda) \hat{D}(z) \hat{D}^\dagger(\lambda) = \hat{D}(z) \exp(-z \lambda^* + z^* \lambda),$$

We simplify this expression as follows: By using

$$\begin{aligned} z\hat{b}^\dagger(t) - z^*\hat{b}(t) &= i \int dk k w_q(k) [(z^* \cosh r_k - z \sinh r_k) \hat{a}_k(t) + (z \cosh r_k - z^* \sinh r_k) \hat{a}_k^\dagger(t)] \\ &= \int dk \left[Z_k(z, t) \hat{a}_k^\dagger - Z_k^*(z, t) \hat{a}_k \right], \end{aligned} \quad (73)$$

with

$$Z_k(z, t) := ik w_q(k) (z \cosh r_k - z^* \sinh r_k) e^{ik(t+x_A)}, \quad (74)$$

the displacement operator for the local mode $\hat{D}_{b(t)}(z) = e^{z\hat{b}^\dagger(t) - z^*\hat{b}(t)}$ can be written as a product of the displacement operator for each k mode of the original field operator:

$$\begin{aligned} \hat{D}_{b(t)}(z) &= \prod_k \exp \left[Z_k(z, t) \hat{a}_k^\dagger - Z_k^*(z, t) \hat{a}_k \right] \\ &= \prod_k \hat{D}_{a_k}(Z_k(z, t)). \end{aligned} \quad (75)$$

Therefore, the projector (72) can be expressed by the displacement operator for each k mode of the original field operator.

D. Quasi-probability

Let us consider the quasi-probability with the initial vacuum state $\hat{\rho}_0 = |g\rangle\langle g|$ in a quantum field. The quasi-probability was evaluated as follows:

$$\begin{aligned} q_{s_1 s_2} &= \text{Re} \langle g | \hat{M}_{s_2}(t_2) \hat{M}_{s_1}(t_1) | g \rangle \\ &= \frac{(1-s_1)(1-s_2)}{4} + \frac{(1-s_2)s_1}{2\pi} \text{Re} \int dz e^{-|z|^2/2 - \beta^* z + \beta z^*} \langle g | \hat{D}_{b_1}(z) | g \rangle \\ &\quad + \frac{(1-s_1)s_2}{2\pi} \text{Re} \int dz e^{-|z|^2/2 - \beta^* z + \beta z^*} \langle g | \hat{D}_{b_2}(z) | g \rangle \\ &\quad + \frac{s_1 s_2}{\pi^2} \text{Re} \int d^2 z_2 d^2 z_1 e^{-|z_2|^2/2 - \beta^* z_2 + \beta z_2^*} e^{-|z_1|^2/2 - \beta^* z_1 + \beta z_1^*} \langle g | \hat{D}_{b_2}(z_2) \hat{D}_{b_1}(z_1) | g \rangle \\ &= \frac{(1-s_1)(1-s_2)}{4} + \frac{(1-s_2)s_1}{2\pi} \text{Re}[I_1] + \frac{(1-s_1)s_2}{2\pi} \text{Re}[I_2] + \frac{s_1 s_2}{\pi^2} \text{Re}[I_3], \end{aligned} \quad (76)$$

where integrals I_1 , I_2 , and I_3 are defined as follows:

$$I_{1,2} = \int d^2 z e^{-|z|^2/2 - \beta^* z + \beta z^*} \langle g | \hat{D}_{b_{1,2}}(z) | g \rangle, \quad (77)$$

$$I_3 = \int d^2 z_2 d^2 z_1 e^{-|z_2|^2/2 - \beta^* z_2 + \beta z_2^*} e^{-|z_1|^2/2 - \beta^* z_1 + \beta z_1^*} \langle g | \hat{D}_{b_2}(z_2) \hat{D}_{b_1}(z_1) | g \rangle. \quad (78)$$

By using the relation (75), the expectation values in integrals I_1 , I_2 , and I_3 are evaluated as

$$\begin{aligned} \langle g | \hat{D}_{b(t)}(z) | g \rangle &= \prod_k \langle g | \hat{D}_{a_k}[Z_k(z, t)] | g \rangle = \prod_k \exp \left[-\frac{1}{2} |Z_k(z, t)|^2 \right] \\ &= \exp \left[-\frac{1}{2} \int dk k^2 w_q^2(k) |z \cosh r_k - z^* \sinh r_k|^2 \right] \\ &= \exp \left[-\frac{x^2 + \ell^2 \omega^2 y^2}{\pi^{1/2} \ell \omega} \right], \end{aligned} \quad (79)$$

$$\begin{aligned} \langle g | \hat{D}_{b_2}(z_2) \hat{D}_{b_1}(z_1) | g \rangle &= \prod_k \langle g | \hat{D}_{a_k}[Z_k(z_2, t_2)] \hat{D}_{a_k}[Z_k(z_1, t_1)] | g \rangle \\ &= \prod_k \exp \left[\frac{1}{2} \left(Z_k(z_2, t_2) Z_k^*(z_1, t_1) - Z_k^*(z_2, t_2) Z_k(z_1, t_1) \right) \right] \langle g | \hat{D}_{a_k}[Z_k(z_2, t_2) + Z_k(z_1, t_1)] | g \rangle \\ &= \prod_k e^{\frac{1}{2} (Z_2 Z_1^* - Z_2^* Z_1)} e^{-\frac{1}{2} (Z_1 + Z_2)(Z_1 + Z_2)^*} \\ &= \prod_k \exp \left[-k^2 w_q^2(k) \left(\frac{|z_1 \cosh r_k - z_1^* \sinh r_k|^2}{2} + \frac{|z_2 \cosh r_k - z_2^* \sinh r_k|^2}{2} \right. \right. \\ &\quad \left. \left. + e^{-ik t_{21}} (z_2^* \cosh r_k - z_2 \sinh r_k)(z_1 \cosh r_k - z_1^* \sinh r_k) \right) \right] \\ &= \exp \left[-\frac{2\ell^3}{\pi^{1/2} \omega} \int dk k e^{-\ell^2 k^2} [k^2 (x_1^2 + x_2^2) + \omega^2 (y_1^2 + y_2^2) \right. \\ &\quad \left. + 2e^{-ik t_{21}} (kx_1 + i\omega y_1)(kx_2 - i\omega y_2)] \right] \\ &=: \exp(-I_4), \end{aligned} \quad (80)$$

where $z_{1,2} = x_{1,2} + iy_{1,2}$ and $t_{21} = t_2 - t_1$. The integral I_4 is

$$\begin{aligned} I_4 &= \frac{1}{4\ell^4 \omega} \left[\frac{\ell}{\pi^{1/2}} \left\{ -2t_{21}^2 x_1 x_2 + 4\ell^4 (y_1 + y_2)^2 \omega^2 + 4\ell^2 ((x_1 + x_2)^2 + t_{21}(x_1 y_2 - x_2 y_1) \omega) \right\} \right. \\ &\quad \left. - e^{-\frac{t_{21}^2}{4\ell^2}} \left\{ -t_{21}^3 x_1 x_2 + 2\ell^2 t_{21} (3x_1 x_2 + t_{21} x_2 y_1 \omega - t_{21} x_1 y_2 \omega) + 4\ell^4 \omega (-x_2 y_1 + y_2 x_1 + t_{21} y_1 y_2 \omega) \right\} \right. \\ &\quad \left. \times \left(i + \text{Erfi} \left[\frac{t_{21}}{2\ell} \right] \right) \right]. \end{aligned} \quad (81)$$

Therefore, I_1 , I_2 , and I_3 become

$$I_{1,2} = \frac{\pi}{\sqrt{1/2 + \frac{1}{\pi^{1/2} \ell \omega}} \sqrt{1/2 + \frac{\ell \omega}{\pi^{1/2}}}} \exp \left(-\frac{\beta^2}{1/2 + \ell \omega / \pi^{1/2}} \right), \quad (82)$$

$$I_3 = \int d^2 z_2 d^2 z_1 e^{-|z_2|^2/2 - \beta^* z_2 + \beta z_2^*} e^{-|z_1|^2/2 - \beta^* z_1 + \beta z_1^*} \exp(-I_4(z_1, z_2)). \quad (83)$$

After performing a Gaussian integral with respect to z_1 and z_2 in I_3 , we obtain the exact formula for $q_{s_1 s_2}$ (Eq. (76)). The resulting expression has a rather complicated form and we do not present it here. The quasi-probability depends on the parameters through a combination of $\omega \ell$ and t_{21} / ℓ .

Figures 13 and 14 show the negative regions of the quasi-probabilities q_{++} and q_{--} in the (t_{21}, β) plane with values of $\omega \ell = 0.4\text{--}4$. The structures of the negative regions of q_{++} and q_{--} for the quantum field are similar to those for the harmonic oscillator case, such as the fringe structure of q_{++} and the violation of q_{--} near $\beta \sim 0$. The major difference is the loss of periodicity in the time direction. Indeed, in q_{++} and q_{--} , the symmetry around half of the period with respect to time on the horizontal axis, which is exhibited in the case of harmonic oscillators, is lost. The loss of time periodicity is related to the mixedness of the local mode defined by the quantum field; as the local mode is a subsystem embedded in a total pure system, its state inevitably becomes mixed. This mixedness depends on

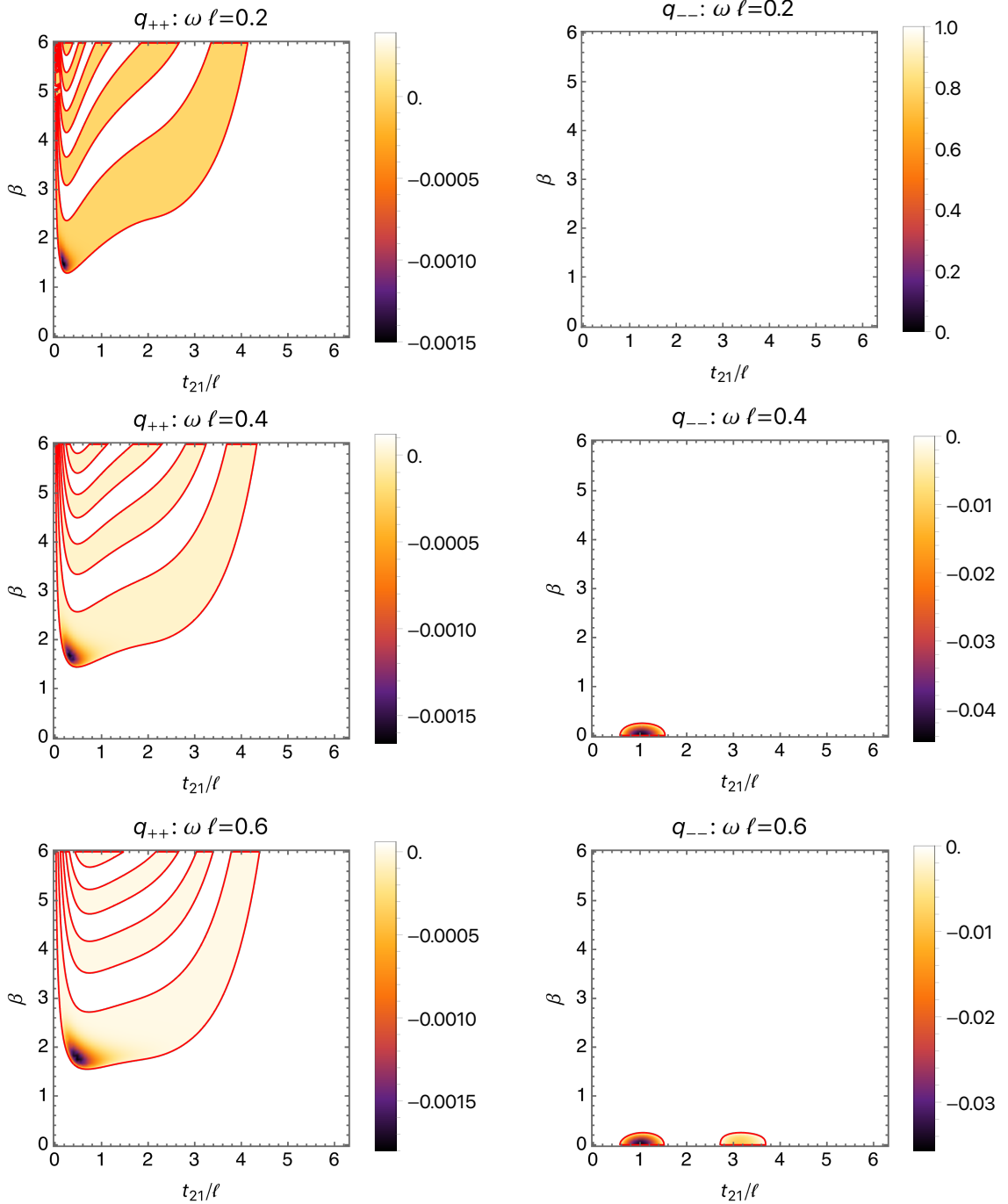


FIG. 13. Negative regions of the quasi-probability (enclosed by red lines) for the local mode of the quantum field. The quasi-probabilities q_{++} and q_{--} with $\omega\ell = 0.2, 0.4$, and 0.6 are shown.

the size of the local region and the UV cutoff length and reflects the entanglement between the local mode and its complementary degrees of freedom. The evolution of the local mode is nonunitary; Therefore, the periodicity of the state in the time direction is lost. However, the Fourier modes (k -mode) are decoupled each other in the Fourier space and the local mode can be expressed as the sum of the decoupled Fourier modes. The loss of periodic features is explained by a dephasing effect.

It is worth mentioning that regions with a negative q_{--} disappear when $\omega\ell$ is too large or too small. This behavior can be explained by the fact that $\omega\ell$ corresponds to the squeezing parameter of the coherent squeezing measurement of the harmonic oscillator. Because the typical wavenumber of the local mode is $k \sim 1/\ell$, we can regard the parameter

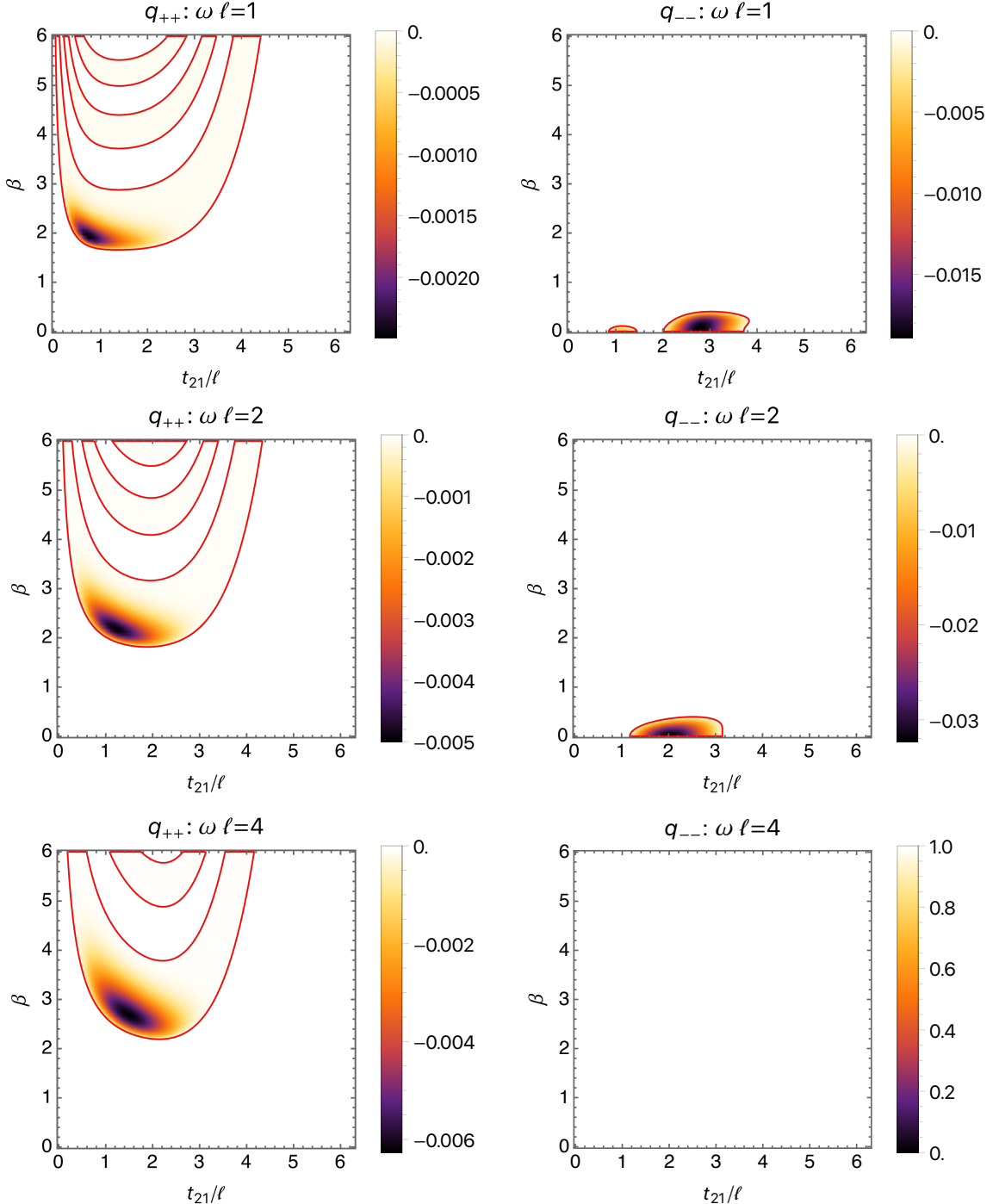


FIG. 14. Negative regions of the quasi-probability (enclosed by red lines) for the local mode of the quantum field. The quasi-probabilities q_{++} and q_{--} with $\omega\ell = 1, 2$, and 4 are shown.

$\omega\ell$ as an effective squeezing parameter by comparing (17) and (68). Hence, when $\omega\ell$ is too large or too small, too little information is obtained from the measurements (left and right panels in Fig. 11). Therefore, the quantum nature of the measurement is not visible and the LGIs are not violated. For q_{++} , the negative value of the quasi-probability approaches zero as squeezing ($\sim\omega\ell$) increases, which is similar to the harmonic oscillator in the previous section. However, the difference is that the negative regions shift toward larger positive values of β as squeezing increases significantly, although we did not explicitly demonstrate this.

IV. SUMMARY AND CONCLUSION

We showed violations of the LGIs in terms of the two-time quasi-probability using Gaussian (squeezed) coherent projectors for a harmonic oscillator and a chiral scalar field. For the harmonic oscillator, violations appear mainly in q_{++} and q_{--} even in vacuum. In the thermal state, the LGIs are not violated when the temperature is sufficiently high. When the projector is prepared in a squeezed coherent state, the quasi-probability reaches -0.123 for $r \sim 0.31$ and $\beta \sim 0.57$, which is equivalent to 98% of the Lüders bound. Generally, a violation of LGIs occurs when the measurement results differ from those classically expected. Therefore, the violation of LGIs represents a feature of the quantumness of the systems; however, further study is required to clarify why a violation close to the Lüders bound is obtained.

We also showed violations of the LGIs for a local mode in the chiral scalar field, similar to those for the harmonic oscillator. A major difference is the disappearance of the periodicity in violations. The reason for this periodicity loss is that the local mode is in a mixed state as a subsystem of the entire system. This is consistent with previous results [15]. This could be related to the entanglement entropy of the local mode. The violations of the LGI observed here are more significant than those with the simple projection operators reported in Tani *et al.* [15].

Our results can be applied to experiments on LGIs using a quantum Hall edge system [20]. Because we use the Gaussian POVM measurement of local modes, we should obtain a dichotomic value of $\hat{Q}(t) = s(2\hat{M}_s(t) - 1)$ by measuring (q, p) , where \hat{M}_s is given by Eq. (69). To this end, we consider adjacent regions A and B and measure their local values q_A and q_B using the window function $w_q(x)$: $\hat{q}_A = \int dx w_q(x - x_A) \hat{\Pi}(t + x)$ and $\hat{q}_B = \int dx w_q(x - x_A - \ell) \hat{\Pi}(t + x) = \int dx w_q(x - x_A) \hat{\Pi}(t + x + \ell)$, where the window function is defined by (66). Using \hat{q}_A and \hat{q}_B , which include the information of the momentum because their difference is equivalent to the momentum essentially, makes it possible to obtain Q to perform a coherent measurement (69).

As well as an application of our theoretical predictions to quantum Hall experiments, applying them to harmonic oscillator systems would also be interesting. Recently, macroscopic oscillators have attracted attention as a means to explore the boundary between the worlds of quantum and classical mechanics (e.g., [22–24]). In such macroscopic oscillators, techniques such as continuous measurements, feedback control, and optimal filters are used to generate quantum states. There is also the issue of constructing dichotomic measurements in macroscopic oscillators. Therefore, applying our predictions to such systems is not trivial and further investigation is necessary.

ACKNOWLEDGMENTS

We thank Masahiro Hotta for providing valuable insight into this subject. Y.N. was supported by JSPS KAKENHI (Grant Nos. JP22H05257 and JP19K03866). A.M. was supported by JSPS KAKENHI (Grant Nos. JP23K13103 and JP23H01175). K.Y. was supported by JSPS KAKENHI (Grant Nos. JP22H05263 and JP23H01175).

Appendix A: Another derivation of $q_{s_1 s_2}$ with a squeezed coherent-state projector

We can derive (29) without using the properties of the squeezed coherent state. The initial vacuum state is considered as follows:

$$\hat{\rho}_0 = |0_a\rangle\langle 0_a|. \quad (\text{A1})$$

The measurement operator with the “vacuum” seed state is

$$\begin{aligned} \hat{M}_s(t) &= \frac{1-s}{2} + s\hat{D}_{b(t)}(\beta)|0_{b(t)}\rangle\langle 0_{b(t)}|\hat{D}_{b(t)}^\dagger(\beta) \\ &= \frac{1-s}{2} + \frac{s}{\pi} \int d^2z e^{-|z|^2/2} \hat{D}_{b(t)}(\beta)\hat{D}_{b(t)}(z)\hat{D}_{b(t)}^\dagger(\beta) \\ &= \frac{1-s}{2} + \frac{s}{\pi} \int d^2z e^{-|z|^2/2 - \beta^*z + \beta z^*} \hat{D}_a[Z(t, z)], \end{aligned} \quad (\text{A2})$$

where $Z(t, z) = (z \cosh r - z^* \sinh r)e^{i\Omega t}, e^{2r} = \omega/\Omega$. The quasi-probability is

$$\begin{aligned} q_{s_1 s_2} &= \text{Re} \langle 0_a | \hat{M}_{s_2}(t_2) \hat{M}_{s_1}(t_1) | 0_a \rangle \\ &= \frac{(1-s_1)(1-s_2)}{4} + \frac{(1-s_2)s_1}{2\pi} \int d^2 z_1 e^{-|z_1|^2/2 - \beta^* z_1 + \beta z_1^*} \langle \hat{D}_a[Z(t_1, z_1)] \rangle \\ &\quad + \frac{(1-s_1)s_2}{2\pi} \int d^2 z_2 e^{-|z_2|^2/2 - \beta^* z_2 + \beta z_2^*} \langle \hat{D}_a[Z(t_2, z_2)] \rangle \\ &\quad + \frac{s_1 s_2}{\pi^2} \text{Re} \int d^2 z_1 d^2 z_2 e^{-|z_1|^2/2 - \beta^* z_1 + \beta z_1^* - |z_2|^2/2 - \beta^* z_2 + \beta z_2^*} \langle \hat{D}_a[Z(t_2, z_2)] \hat{D}_a[Z(t_1, z_1)] \rangle. \end{aligned} \quad (\text{A3})$$

The expected values of the displacement operators are

$$\langle \hat{D}_a[Z(t_1, z_1)] \rangle = \langle \hat{D}_a[Z(t_2, z_2)] \rangle = \exp \left(-\frac{1}{2} |z \cosh r - z^* \sinh r|^2 \right), \quad (\text{A4})$$

$$\begin{aligned} \langle \hat{D}_a[Z(t_2, z_2)] \hat{D}_a[Z(t_1, z_1)] \rangle &= \langle \hat{D}_a[Z(t_1, z_1) + Z(t_2, z_2)] \rangle \exp \left[\frac{1}{2} (Z_2 Z_1^* - Z_1 Z_2^*) \right] \\ &= \exp \left(-\frac{|Z_1|^2}{2} - \frac{|Z_2|^2}{2} - Z_1 Z_2^* \right). \end{aligned} \quad (\text{A5})$$

After performing the Gaussian integrals in (A3), we obtain $q_{s_1 s_2}$ using the squeezed coherent-state projector.

-
- [1] A. J. Leggett and A. Garg, Quantum mechanics versus macroscopic realism: Is the flux there when nobody looks?, *Phys. Rev. Lett.* **54**, 857 (1985).
- [2] J. J. Halliwell, Necessary and sufficient conditions for macrorealism using two- and three-time leggett-garg inequalities, *Journal of Physics: Conference Series* **1275**, 012008 (2019).
- [3] C. Budroni, T. Moroder, M. Kleinmann, and O. Gühne, Bounding temporal quantum correlations, *Phys. Rev. Lett.* **111**, 1 (2013), arXiv:1302.6223.
- [4] J. Kofler and i. c. v. Brukner, Condition for macroscopic realism beyond the leggett-garg inequalities, *Phys. Rev. A* **87**, 052115 (2013).
- [5] L. Clemente and J. Kofler, Necessary and sufficient conditions for macroscopic realism from quantum mechanics, *Phys. Rev. A* **91**, 062103 (2015).
- [6] L. Clemente and J. Kofler, No fine theorem for macrorealism: Limitations of the leggett-garg inequality, *Phys. Rev. Lett.* **116**, 150401 (2016).
- [7] S. Bose, D. Home, and S. Mal, Nonclassicality of the Harmonic-Oscillator Coherent State Persisting up to the Macroscopic Domain, *Phys. Rev. Lett.* **120**, 210402 (2018).
- [8] C. Mawby and J. J. Halliwell, Leggett-Garg tests for macrorealism in the quantum harmonic oscillator and more general bound systems, *Phys. Rev. A* **105**, 022221 (2022), arXiv:2109.03118.
- [9] C. Mawby and J. J. Halliwell, Leggett-Garg violations for continuous-variable systems with Gaussian states, *Phys. Rev. A* **107**, 032216 (2023), arXiv:2211.10292.
- [10] D. Das, D. Home, H. Ulbricht, and S. Bose, Mass-independent test of quantumness of a massive object, arXiv:2211.10318.
- [11] K. Hatakeyama, D. Miki, M. Tani, Y. Yamasaki, S. Iso, A. Salim Adam, A. Rohim, and K. Yamamoto, Violation of the two-time Leggett-Garg inequalities for a harmonic oscillator, arXiv:2310.16471 (2023).
- [12] A. Asadian, C. Brukner, and P. Rabl, Probing Macroscopic Realism via Ramsey Correlation Measurements, *Phys. Rev. Lett.* **112**, 190402 (2014), arXiv:1309.2229.
- [13] S.-S. Majidy, H. Katiyar, G. Anikeeva, J. Halliwell, and R. Laflamme, Exploration of an augmented set of Leggett-Garg inequalities using a noninvasive continuous-in-time velocity measurement, *Phys. Rev. A* **100**, 042325 (2019), arXiv:1907.05489.
- [14] G. C. Knee, K. Kakuyanagi, M.-C. Yeh, Y. Matsuzaki, H. Toida, H. Yamaguchi, S. Saito, A. J. Leggett, and W. J. Munro, A strict experimental test of macroscopic realism in a superconducting flux qubit, *Nature communications* **7**, 13253 (2016).
- [15] M. Tani, K. Hatakeyama, D. Miki, Y. Yamasaki, and K. Yamamoto, Violation of the two-time Leggett-Garg inequalities for a coarse-grained quantum field, arXiv:2311.02867 (2023).
- [16] J. J. Halliwell, Leggett-garg inequalities and no-signaling in time: A quasiprobability approach, *Phys. Rev. A* **93**, 022123 (2016).
- [17] G. Adesso, S. Ragy, and A. R. Lee, Continuous Variable Quantum Information: Gaussian States and Beyond, *Open Syst. Inf. Dyn.* **21**, 1440001 (2014).
- [18] K. B. Mo/ller, T. G. Jo/rgensen, and J. P. Dahl, Displaced squeezed number states: Position space representation, inner product, and some applications, *Phys. Rev. A* **54**, 5378 (1996).

- [19] D. Yoshioka, *The Quantum Hall Effect* (Springer-Verlag, 2002).
- [20] M. Hotta, Y. Nambu, Y. Sugiyama, K. Yamamoto, and G. Yusa, Expanding edges of quantum Hall systems in a cosmology language: Hawking radiation from de Sitter horizon in edge modes, *Phys. Rev. D* **105**, 105009 (2022), arXiv:2202.03731.
- [21] Y. Nambu and M. Hotta, Analog de Sitter universe in quantum Hall systems with an expanding edge, *Phys. Rev. D* **107**, 085002 (2023), arXiv:2301.09270.
- [22] T. Westphal, H. Hepach, J. Pfaff, and M. Aspelmeyer, Measurement of gravitational coupling between millimetre-sized masses, *Nature* **591**, 225 (2021), arXiv:2009.09546.
- [23] C. Whittle *et al.*, Approaching the motional ground state of a 10-kg object, *Science* **372**, 1333 (2021), arXiv:2102.12665.
- [24] J. G. Santiago-Condori, N. Yamamoto, and N. Matsumoto, Verification of conditional mechanical squeezing for a mg-scale pendulum near quantum regimes, arXiv:2008.10848 (2020).